

Assessing transient changes in the ocean carbon cycle during the last deglaciation through carbon isotope modeling

Hidetaka Kobayashi^{1, 2}, Akira Oka², Takashi Obase², and Ayako Abe-Ouchi²

¹Faculty of Science, Academic Assembly, University of Toyama, 3190 Gofuku, Toyama, 930-8555, Japan.

²Atmosphere and Ocean Research Institute, University of Tokyo, 5-1-5 Kashiwanoha, Kashiwa, 277-8568, Japan.

Abstract.

Atmospheric carbon dioxide concentration ($p\text{CO}_2$) has increased by approximately 80 ppm from the Last Glacial Maximum (LGM) to the late Holocene (last deglaciation). The change in this atmospheric greenhouse gas is recognized as a climate system response to gradual change in insolation. Previous modeling studies suggested that the deglacial increase in atmospheric $p\text{CO}_2$ is primarily attributed to the release of CO_2 from the ocean. Additionally, it has been suggested that abrupt change in the Atlantic Meridional Overturning Circulation (AMOC) and associated interhemispheric climate changes are involved in the release of CO_2 . However, understanding remains limited regarding oceanic circulation changes, and the factors responsible for changes in chemical tracers in the ocean of the last deglaciation and their impact on atmospheric $p\text{CO}_2$. We conducted a transient numerical experiment on In this study, we investigated the evolution of the ocean carbon cycle during the last deglaciation. We used a (21 to 11 ka BP) using three-dimensional ocean field from a transient climate model MIROC4m fields from the transient simulation of the last deglaciation as input to an ocean biogeochemical MIROC 4m climate model, which allowed us to evaluate the effects of the gradual warming and the abrupt climate changes associated with the Atlantic Meridional Overturning Circulation during the last deglaciation.

During exhibits abrupt AMOC changes similar to those observed in reconstructions. We validate the simulated ocean carbon cycle changes, and examine possible biases and missing or underestimated processes in the model by comparing simulated carbon isotope ratios with sediment core data. Qualitatively, the modeled changes in atmospheric $p\text{CO}_2$ are consistent with ice core records. For example, during Heinrich Stadial 1 (HS1), the atmospheric partial pressure of carbon dioxide (atmospheric $p\text{CO}_2$) increased as a result of rising sea surface temperature. Subsequently, increases by 10.2 ppm, followed by reduction of 7.0 ppm during the Bølling-Allerød period, characterized by a rapid strengthening of the Atlantic Meridional Overturning Circulation (AMOC), atmospheric $p\text{CO}_2$ showed a decreasing trend. Our decomposition analysis indicates that the declining atmospheric $p\text{CO}_2$ in response to the enhanced AMOC during the BA period were primarily driven by an increase in ocean surface alkalinity, although this effect was partially offset by changes in sea surface temperature.

Meantime, we found that our model generally underestimated (BA) period, and then increase of 6.8 ppm during the Younger Dryas (YD) period. However, the model underestimates the changes in atmospheric $p\text{CO}_2$ changes compared to the during these events compared to values derived from ice core data. To understand this, we conducted an analysis of ocean circulation and water masses using radiocarbon and stable carbon Radiocarbon and stable isotope signatures ($\Delta^{14}\text{C}$ and $\delta^{13}\text{C}$). We found that the overall changes in the deep water $\Delta^{14}\text{C}$ in response to the AMOC change are quantitatively consistent with

the sediment core data. However, the model underestimates the increased ventilation in the deep ocean and the indicate that the model underestimates both the activated deep ocean ventilation and reduced efficiency of biological carbon export in the Southern Ocean during mid-HS1 compared to estimates derived from sediment core data. In addition, the model underestimates , and the active ventilation in the North Pacific Intermediate Water during mid-HS1, as suggested by sediment core data. These underestimations in the activation of the deep ocean circulation and the limitation of biological productivity could be the primary reasons why our model exhibits smaller atmospheric $p\text{CO}_2$ changes than ice core data.

Our decomposition analysis, which estimates the quantitative contribution to the oceanic $p\text{CO}_2$, suggests that changes in alkalinity have played a central role in driving variations and trends in atmospheric HS1. The relatively small changes in simulated atmospheric $p\text{CO}_2$ as during HS1 might be attributable to these underestimations of ocean circulation variation. The changes in $\Delta^{14}\text{C}$ associated with strengthening and weakening of the AMOC during the BA and YD periods are generally consistent with values derived from sediment core records. However, although the data indicate continuous increase in $\delta^{13}\text{C}$ in the deep ocean circulation changes. This finding may provide valuable insights into the model-dependent response of the ocean carbon cycle to changes in the AMOC, as several previous studies have emphasized the importance of throughout the YD period, the model shows the opposite trend. It suggests that the model either simulates excessive weakening of the AMOC during the YD period, or has limited representation of geochemical processes, including marine ecosystem response and terrestrial carbon storage. Decomposing the factors behind the changes in ocean $p\text{CO}_2$ reveals that variations in temperature and alkalinity have the AMOC in influencing changes greatest impact on change in atmospheric $p\text{CO}_2$. Compensation for the effects of temperature and alkalinity suggests that the AMOC changes and the associated bipolar climate changes contribute to the slight decrease (increase) in atmospheric $p\text{CO}_2$, but the magnitude and direction of these changes have varied widely between studies during the BA (YD) period.

Copyright statement. TEXT

1 Introduction

The Earth's climate has transitioned from the cold climatic shifted from the colder conditions of the Last Glacial Maximum (LGM) , which is approximately 21,000 years ago, to the warmer conditions of the Holocene. This climatic transition, known as the last deglaciation, was accompanied by an increase in the atmospheric partial pressure occurred approximately 21 to 11 ka BP (thousand years before present). During this period, the atmospheric concentration of carbon dioxide ($p\text{CO}_2$) of nearly 90 increased by almost 80 ppm (Barnola et al., 1987; Petit et al., 1999; Siegenthaler et al., 2005; Jouzel et al., 2007; Lüthi et al., 2008). The changes in the carbon cycle leading to changes that affect the variation in atmospheric $p\text{CO}_2$ are thought to be closely linked to the climate changes that occurred during the deglaciation period closely related to the changes in climate observed during the last deglaciation.

In attempting to elucidate the mechanisms of climate change on the glacial–interglacial scale, previous modeling studies mainly focused on assessing the steady-state difference between the LGM and the preindustrial period. With the development of computational tools, transient climate modeling of the last glacial termination has recently been conducted, using temporal changes in insolation, greenhouse gas concentrations derived from ice core records, and meltwater fluxes from ice sheets (Lunt et al., 2006; Timm and Timmermann, 2007; Liu et al., 2009; He et al., 2013; Ganopolski and Roche, 2009; Menviel et al., 2011; Iva . Transient climate modeling has distinct advantages because it avoids unrealistic equilibrium assumptions and it includes climate responses to internal variability or abrupt change. It also facilitates direct comparison between models and proxies, thereby allowing identification of temporal leads or lags in the process with respect to forcing. In these transient climate modeling studies, changes in atmospheric $p\text{CO}_2$, a greenhouse gas, are applied as external forcing. However, understanding the feedback between the climate and the carbon cycle is critical for understanding the long-term changes in climate dynamics. As fundamental research guided by this perspective, earlier modeling studies examined the temporal changes in the ocean carbon cycle during the last deglaciation or late Pleistocene, including glacial–interglacial cycles, using Earth System Models of Intermediate Complexity, e.g., CLIMBER-2 (Bouttes et al., 2012a; Brovkin et al., 2012; Mariotti et al., 2016; Ganopolski and Brovkin, 20 , Bern 3D (Tschumi et al., 2011; Menviel et al., 2012; Pöppelmeier et al., 2023) and LOVECLIM (Menviel et al., 2018; Stein et al., 2020) . Generally, the increase in sea surface temperature (SST) and the reduction in the expansion of carbon-rich Antarctic Bottom Water (AABW), together with changes in the characteristics of the biological carbon pump and carbonate chemistry, are considered key processes that contributed to the increase in atmospheric $p\text{CO}_2$ during the last deglaciation (Brovkin et al., 2012; Menviel et

~~The concentrations-~~ Those earlier studies greatly advanced our understanding of changes in both the climate and the carbon cycle on scales of thousands to tens of thousands of years. However, the mechanisms behind the observed increase in atmospheric $p\text{CO}_2$ during the glacial termination are not fully understood. It has been suggested that release of carbon from the deep Southern Ocean to the atmosphere might have played a role in the rapid increase in atmospheric $p\text{CO}_2$ during the last deglaciation (Tschumi et al., 2011; Bouttes et al., 2012a; Mariotti et al., 2016; Menviel et al., 2018; Stein et al., 2020; Sigman et al., 2021) . The release of CO_2 can be triggered by disruption of the stratification in the Southern Ocean and change in the deep ocean circulation, which can be affected by westerly winds in the Southern Hemisphere, freshwater input from the Antarctic ice sheet, and brine rejection around Antarctica. It has also been suggested that variation in North Pacific Intermediate Water (NPIW), associated with changes in the Atlantic Meridional Overturning Circulation (AMOC), might have contributed to the observed increase in atmospheric $p\text{CO}_2$ (Okazaki et al., 2010; Menviel et al., 2014).

To clarify the mechanisms behind long-term changes in ocean dynamics, the concentration or isotopic composition of elements in seawater can provide information on the processes responsible for their distribution. ~~Therefore~~ Thus, analysis of geochemical proxies in paleoclimatological archives can help oceanographers gain insight into past ocean variability and its underlying mechanisms.

Stable and radioactive carbon isotopes of dissolved inorganic carbon (DIC) in seawater are representative ~~chemical tracers in the ocean~~ oceanic chemical tracers. In seawater, ~~carbon of lighter isotopes is preferentially absorbed during photosynthesis~~ -leading to its accumulation- lighter carbon isotopes are preferentially taken up by phytoplankton during photosynthesis and

they accumulate in the deep ocean as organic matter ~~undergoes degradation is degraded~~ (O'Leary, 1981; Broecker and Maier-Reimer, 1992; Schmittner et al., 2013). ~~Therefore, Anomalies in~~ the stable carbon ~~isotopic-isotope~~ signature ($\delta^{13}\text{C}$) ~~produced by the biological carbon pump spread globally in association with the deep ocean circulation. Therefore, the $\delta^{13}\text{C}$ value differs among water masses within the ocean interior. Radiocarbon (^{14}C) is introduced into seawater through gas exchange at the ocean surface and, and it subsequently decreases in concentration as a result of the through~~ radioactive decay of ^{14}C . Therefore, the radiocarbon ~~isotopic-isotope~~ signature ($\Delta^{14}\text{C}$) serves as an indicator of the deep water flow rate (Stuiver et al., 1983). ~~Recent efforts to compile sediment core records have provided valuable insights into the temporal evolution of the basin-scale distributions of-~~

~~Previous modeling studies examined the processes responsible for glacial–interglacial changes in the distribution of $\delta^{13}\text{C}$ and $\Delta^{14}\text{C}$ (Zhao et al., 2018; Rafter et al., 2022) and (Kurahashi-Nakamura et al., 2017; Menviel et al., 2017; Muglia et al., 2018; Wilmes et al., 2023). It is generally assumed that deep water originating from the Southern Ocean with low $\delta^{13}\text{C}$ (Muglia et al., 2023) during the last deglaciation and $\Delta^{14}\text{C}$ expanded into the deep Atlantic Ocean during the LGM. It is proposed that the carbon isotope distribution during the LGM can be better explained by considering an effective biological pump associated with iron fertilization in the Southern Ocean and a shallower AMOC (Kobayashi et al., 2021).~~

Other proxies used to ~~inter-infer~~ past water mass distribution and deep ~~circulation include neodymium isotope ratios ocean circulation include the neodymium isotope ratio~~ (ϵNd) and the protactinium–thorium ~~ratios-ratio~~ ($^{231}\text{Pa}/^{230}\text{Th}$). ~~Neodymium isotope ratios~~ The ϵNd ratio can be used as a proxy for basin-scale water mass structure because the ~~end-members endmembers~~ differ in each ~~deep water formation region (Howe et al., 2016). Sedimentary water mass source region (Lippold et al., 2012; Howe et al., 2012). The sedimentary $^{231}\text{Pa}/^{230}\text{Th}$ ratios, employed ratio, used~~ as a proxy for ~~changes in flow rates, suggest change in flow rate, suggests~~ that the strength of the ~~Atlantic Meridional Overturning Circulation (AMOC) may AMOC might~~ have changed markedly during the last deglaciation (McManus et al., 2004; Ng et al., 2018). Changes in the AMOC ~~can~~ influence the climatic state by ~~affecting both altering not only the~~ meridional interhemispheric heat transport ~~and, but also~~ the ocean carbon cycle ~~, which in turn regulates and associated changes in~~ atmospheric $p\text{CO}_2$ (Schmittner and Galbraith, 2008; Menviel et al., 2008; Bouttes et al., 2012b). Nevertheless, there is ~~an ongoing debate about ongoing debate regarding~~ the magnitude and ~~direction of changes the direction of the change~~ in atmospheric $p\text{CO}_2$ associated with AMOC ~~variations-variation~~ (Gottschalk et al., 2019).

~~Previous modeling studies examined those processes responsible for Several earlier modeling studies attempted to estimate AMOC variation by examining changes in the distribution of carbon isotope signature (Schmittner and Lund, 2015; Pöppelmeier et al., 2023). By estimating the AMOC that best fits the model and the data for $\delta^{13}\text{C}$ and $\Delta^{14}\text{C}$ in glacial oceans (Kurahashi-Nakamura et al., 2017; Menviel et al., 2023). Changes in the efficiency of biological carbon pumps and the deep ocean circulation are recognized as key factors contributing to variations in carbon isotope signatures. However, it is worth noting that previous modeling studies have been somewhat limited in scope, focusing primarily on assessing steady-state differences between the LGM and the preindustrial period. Clarifying the factors behind changes in the distribution of chemical tracers during the glacial termination will improve (Schmittner and Lund, 2015) or $\delta^{13}\text{C}$ and multiple chemical tracers in seawater (Pöppelmeier et al., 2023), those studies improved our understanding of the variability of the ocean carbon cycle and climate during this period.~~

Transient climate model simulations for the last deglaciation period have been conducted, considering prescribed temporal changes in insolation, greenhouse gas concentrations derived from ice core records, and meltwater fluxes from ice sheets (Lunt et al., 2006; Timm and Timmermann, 2007; Liu et al., 2009; He et al., 2013; Ganopolski and Roche, 2009; Menviel et al., 2011; Iva
130 ~~-. The temporal evolution of~~ relationship between changes in the AMOC and the ocean carbon cycle during the last deglaciation has been examined using Earth System Models of Intermediate Complexity (EMIC), e.g., CLIMBER-2 (Bouttes et al., 2012a; Brovkin et al., 2012), Bern 3D (Tschumi et al., 2011; Menviel et al., 2012; Pöppelmeier et al., 2023) and LOVECLIM (Menviel et al., 2018; Stein et al., 2020). Other related studies have attempted to estimate variations in the AMOC with respect to meltwater input to the oceans
135 by analyzing changes in carbon isotopic signatures (Schmittner and Lund, 2015; Gu et al., 2021; Pöppelmeier et al., 2023). Generally, the increase in sea surface temperature (SST) and the reduction in the expansion of carbon-rich Antarctic Bottom Water (AABW), along with changes in the characteristics of biological carbon pumps and carbonate chemistry, are considered key processes that contributed to the increase in atmospheric $p\text{CO}_2$ during early deglaciation. In recent years, compilation of many sediment core records covering the last deglaciation (Brovkin et al., 2012; Menviel et al., 2012). Several related studies
140 have suggested that the release of carbon from the deep Southern Ocean to the atmosphere, induced by disruption of the stratification in the Southern Ocean and changes in deep ocean circulation driven by westerly winds in the Southern Hemisphere, freshwater input from the Antarctic ice sheet, and brine rejection around Antarctica, may have been a potential driver of the rapid increase in atmospheric $p\text{CO}_2$ during the last deglaciation (Tschumi et al., 2011; Bouttes et al., 2012a; Mariotti et al., 2016; Menviel et al., 2016). It is also suggested that variation of the North Pacific Intermediate Water (NPIW), associated with changes in the circulation
145 of the Atlantic Ocean, may have contributed to the increase in atmospheric $p\text{CO}_2$ (Okazaki et al., 2010; Menviel et al., 2014). Some of these EMIC studies have discussed the mechanisms of has deepened our understanding of the spatiotemporal changes in carbon isotope ratios during this period (Zhao et al., 2018; Rafter et al., 2022; Muglia et al., 2023; Skinner et al., 2023). By comparing the compiled data with model output, it has been possible to gain valuable insights into deglacial changes in the ocean carbon cycle by conducting model-data comparisons of carbon isotope signatures. However, these discussions are limited
150 to the vertical one-dimensional distribution of these signatures.

To investigate the causes of changes in carbon isotope signatures, this study conducted a transient model experiment In this study, we conducted transient model experiments of the ocean carbon cycle and compared the model results with a recently compiled sediment core record records to investigate the mechanisms of deglacial changes in carbon isotope signatures. Additionally, the factors responsible for we analyzed the drivers of the changes in atmospheric $p\text{CO}_2$ resulting from variation in ocean carbon storage were analyzed. The objective variations in the ocean carbon cycle. The objectives of this study is to gain a better understanding of the processes contributing to changes in the were to clarify the reproducibility of deglacial carbon cycle through these efforts changes in the model, understand the mechanisms underlying these changes, and identify the processes that are missing or underestimated in the model.

2 Methods

160 2.1 Model

~~This study performed numerical experiments by coupling an~~ In this study, numerical experiments on the ocean carbon cycle were performed using an offline ocean biogeochemical tracer model based on Parekh et al. (2005) ~~with~~ within the framework of the CCSR Ocean Component Model version 4.0 (Hasumi, 2006) ~~to evaluate the transient response of the global ocean carbon cycle during the last deglaciation. The~~. The model has an approximate horizontal resolution of ~~the model was approximately~~ 1 degree, and it ~~had~~ includes 44 vertical layers (~~with thicknesses ranging from 5 to 250 m~~). ~~The boundary condition of the~~. The ocean biogeochemical cycle model ~~was the~~ is forced with monthly averaged output ~~of from~~ a climate model simulation ~~focused on designed specifically for~~ the last deglaciation (Obase and Abe-Ouchi, 2019; Obase et al., 2021) ~~performed using an and run with the MIROC 4m atmosphere–ocean general circulation model (AOGCM) ,i.e., MIROC 4m (K-I Model Developers, 2004) ,incorporating~~ (Obase and Abe-Ouchi, 2019; Obase et al., 2021). The boundary conditions include horizontal advection velocity, sea surface height, vertical diffusivity, temperature, salinity, shortwave radiation, wind speed above the sea surface, and sea ice concentration. ~~The prognostic~~ Prognostic variables for the ocean biogeochemical ~~model were~~ cycle model include phosphate, DIC, alkalinity, dissolved organic phosphate, dissolved oxygen, iron, silicate, and carbon isotopes of DIC (^{13}C and ^{14}C). The availability of light, phosphate, and iron ~~was is~~ used to determine the rate of phosphate uptake by phytoplankton. ~~Sedimentation~~ Notably, sedimentation processes on the seafloor ~~were are~~ not considered, and all particles reaching the seafloor ~~were are~~ assumed to dissolve in the deepest layer of the model.

2.2 Experimental design

~~We conducted~~ To evaluate the transient response of the global ocean carbon cycle during the last deglaciation, we conducted offline ocean carbon cycle experiments ~~for~~ forced with the outputs of the AOGCM MIROC 4m simulation, covering the period 21 to 11 ka BP. The MIROC 4m simulation focusing on the last deglaciation ~~spanning from~~ was performed according to the PMIP protocol (Ivanovic et al., 2016) with respect to the changes in orbital parameters and greenhouse gases during this period (Obase and Abe-Ouchi, 2019). They fixed the ice sheet to the 21 to 11 thousand years before present (kaBP) ka BP state of the ICE-5G reconstruction. Freshwater inflow from the Northern Hemisphere ice sheets deviates from the PMIP protocol after the latter half of Heinrich Stadial 1 (HS1). This approach seeks to align the simulated AMOC variations with those reconstructed from $^{231}\text{Pa}/^{230}\text{Th}$ sediment core records and the associated climate changes that occurred during the Bølling–Allerød (BA) and Younger Dryas (YD) periods.

2.2.1 Steady-state experiment on the ocean carbon cycle for the Last Glacial Maximum

~~To obtain the initial state of the deglaciation experiment, the~~ The ocean biogeochemical cycle model was ~~spun up~~ initialized through spin-up under the LGM ocean state (21 kaBP ka BP) calculated by the AOGCM. Dust deposition to the ocean surface was taken from a simulation ~~of~~ conducted using the SPRINTARS aerosol transport–radiation model computed under LGM climatic conditions (Takemura, 2005). We assumed ~~that~~ iron deposition at the sea surface ~~to be~~ accounts for 3.5 wt% of the total dust deposition, with an assumed iron solubility of 1% (Parekh et al., 2005), ~~which was derived from the ratio of wet and dry dust deposition and its solubility. However, it should be noted that some uncertainty is associated with these parameters.~~ The

initial distribution of ocean biogeochemical tracers was taken from the climatology of the World Ocean Atlas 2001 (Conkright et al., 2002; Locarnini et al., 2002) and the Global Ocean Data Analysis Project (Key et al., 2004). The initial iron concentration was set to a constant value of 0.6 nmol. The model ~~was is~~ initialized with values of atmospheric $\delta^{13}\text{C}$ and $\Delta^{14}\text{C}$ ~~at 21-kaBP~~ of -6.5‰ and 0‰ respectively.

Notably, the biogeochemical cycle simulation of the LGM ocean performed in this study did not include certain processes such as enhanced Southern Ocean stratification, iron fertilization from glaciogenic dust, and carbonate compensation, as discussed in Kobayashi et al. (2021). These three processes ~~were are~~ found to contribute to the glacial reduction in atmospheric $p\text{CO}_2$ ~~in our previous studies, and therefore,~~ with values of 294.7 ppm for the preindustrial run (PI ~~sed in Kobayashi et al. (2021))~~ and 217.4 ppm for the LGM run (LGM ~~all in Kobayashi et al. (2021))~~). Therefore, the calculated atmospheric $p\text{CO}_2$ during the LGM ~~was is~~ expected to be higher than the atmospheric $p\text{CO}_2$ reported in ~~Kobayashi et al. (2021)~~ ~~Additional Kobayashi et al. (2021)~~. Further experiments with the ocean general circulation model ~~experiments~~ are needed to obtain ~~the physical ocean fields that account a physical ocean field that accounts~~ for the enhanced ~~Southern Ocean stratification; therefore, this process could not be incorporated into the current model setup~~ stratification of the Southern Ocean during glacial periods. Therefore, it was not possible to include this process in the model settings adopted for this study.

2.2.2 Transient experiment on the ocean carbon cycle during the last deglaciation

A transient experiment was conducted to investigate the ocean biogeochemical carbon cycle during the last deglaciation, starting from the initial state of the LGM ~~The temporal variations in (21 ka BP)~~. Figure 1 illustrates the temporal variations of temperature and the AMOC ~~in the output of the AOGCM within the AOGCM output~~ imposed on the ~~boundary conditions are shown in Fig. 1.~~ forcing of the ocean biogeochemical cycle model. During the transient experiment, dust deposition was periodically adjusted every ~~100 years~~ 100 years based on the scaling between the LGM and the Holocene, using the reconstructed dust deposition from the Dome Fuji ice core (Dome Fuji Ice Core Project Members, 2017). Notably, the transient experiment did not ~~consider temporal variation in the ocean volume or the changes in dissolved matter concentration induced by ocean volume change~~ account for temporal variations in ocean volume caused by ice sheet changes and associated changes in mean ocean concentrations of biogeochemical tracers (i.e., nutrients, alkalinity, and DIC). This simplification ~~will be revised in the future~~ must be revisited in future studies.

We also predicted the ^{13}C and ^{14}C contained in atmospheric CO_2 . After the spin-up Upon completion of the LGM ocean, ~~we determined the spin-up, we established a~~ restoring term to prevent drift counteract drifts in $\delta^{13}\text{C}$ and $\Delta^{14}\text{C}$ ~~in the atmosphere due to~~ caused by gas exchange between the atmosphere and the ocean. ~~The restoring term implies~~ This restoring term includes the exchange of carbon isotopes between the atmosphere and the land, together with the production of ^{14}C in the atmosphere. This restoring term was assumed ~~to remain unchanged~~ constant throughout the deglaciation experiment.

3 Results

225 3.1 Ocean LGM time slice of the ocean carbon cycle during the LGM time slice

Figure 2 shows the calculated temporal variations in $\Delta^{14}\text{C}$ -CO₂, $\delta^{13}\text{C}$ -CO₂, and $p\text{CO}_2$ in the atmosphere (solid ~~lines~~), together with their ~~reconstructed estimate (dashed line)~~ estimated values (dashed lines). Figure 2 also shows the temporal variations in the average of $\Delta\Delta^{14}\text{C}$, which are the differences (i.e., the difference in $\Delta^{14}\text{C}$ between the ocean and the atmosphere), $\delta^{13}\text{C}$, and DIC in the middle (500–2000 m) and deep (> 2000 m) layers of the Atlantic, Southern ($<40^\circ\text{S} < 40^\circ\text{S}$), and Pacific oceans. ~~In response to~~ This figure illustrates the changes in the ocean carbon cycle in response to the changing climate and the variation in the deep ocean circulation during the deglaciation, ~~the ocean carbon cycle is altered.~~

~~First, we discuss the~~ Analysis of the modeled differences between the LGM and the Holocene. ~~Our climate model experiment indicates a weaker AMOC~~ indicates that the AMOC is weaker (9.0 Sv) during the LGM (21 kaBP) compared to that in ka BP than during the Holocene (11 kaBP)ka BP, i.e., 17.4 Sv (Figs. 1a and S1). The basin-wide distributions of $\Delta\Delta^{14}\text{C}$ and $\delta^{13}\text{C}$ in the Atlantic and Pacific oceans ~~at specific time during specific~~ periods are presented in Figs. 3 and 4-4, respectively. The model results demonstrate that $\Delta\Delta^{14}\text{C}$, an indicator of ocean ventilation, is lower in the deep Atlantic at 21 ~~kaBP ka BP~~ ka BP than at 11 ~~kaBP ka BP~~ ka BP (Figs. 2c, 3a ~~and f, and 3f~~), which is in qualitative agreement with reconstructions from sediment core records (Rafter et al., 2022). Notably, however, the ~~model experiment underestimates the reconstruction of~~ simulated $\Delta\Delta^{14}\text{C}$ values are less negative than the reconstruction $\Delta\Delta^{14}\text{C}$ values at 21 ~~kaBP ka BP~~ ka BP in the Atlantic below 3000 m and in the Pacific below 2000 m (Fig. 3a).

Regarding $\delta^{13}\text{C}$, the model results show a stronger vertical gradient between the surface and the deep ocean in the Atlantic (Fig. 2h), corresponding to a shallower and weaker AMOC at 21 ~~kaBP ka BP~~ ka BP compared to that at 11 ~~kaBP ka BP~~ ka BP. This qualitative difference is consistent with the reconstructed $\delta^{13}\text{C}$. However, similar to the finding for $\Delta\Delta^{14}\text{C}$, our model experiment underestimates the reconstruction of $\delta^{13}\text{C}$ in the deep ocean, particularly in the Southern ~~and Pacific oceans~~ Ocean (Figs. 2i and ~~j~~ 2j).

Our previous study, which involved numerical experiments under ~~LGM conditions that the climatic conditions of the LGM,~~ and accounted for the enhanced stratification in the Southern Ocean and iron fertilization from glaciogenic dust, showed improved quantitative agreement between the model ~~and results and the~~ sediment core data for dissolved oxygen, $\delta^{13}\text{C}$, and $\Delta^{14}\text{C}$ (Kobayashi et al., 2021). The triangles in Fig. 2 illustrate the changes in the carbon isotope signatures reported in that study. ~~A comparison of the two studies suggests that the absence of these processes is a major factor in the underestimation of~~ Comparison of the results from the two studies highlights the advances made by Kobayashi et al. (2021) in capturing the dynamics of the Southern Ocean, suggesting that incorporation of the processes considered in their research could improve model–data agreement. However, their LGM simulation also slightly overestimated the changes in the carbon isotope signatures in the deep ocean glacial Pacific, and these discrepancies highlight the difficulty of achieving consistent scenarios that account for all changes in the global ocean within a model.

Atmospheric $p\text{CO}_2$ was predicted by running the ocean carbon cycle model. Its value ~~was is~~ 278.1 ppm at 21 ~~kaBP ka BP~~ ka BP and 306.9 ppm at 11 ~~kaBP ka BP~~ ka BP, i.e., a difference of 28.8 ppm, ~~which that~~ is relatively small compared ~~with to~~ the

260 difference of approximately 80 ppm reconstructed from ice cores (approximately 188to–267 ppm in the EPICA Dome C record (Bereiter et al., 2015) and approximately 193to–273 ppm in WAIS Divide the WAIS Divide record (Bauska et al., 2021)). ~~One possible explanation for this discrepancy is~~ This discrepancy could be attributed to several factors, including the relatively small ~~difference in SST~~ differences in SST observed between the two intervals ~~in our experiment~~ (Fig. 1b). ~~Previous studies using~~ Using proxy and data assimilation ~~reported a~~ the global mean SST difference between the LGM and the Holocene ~~of 1.7 to has been reported to be 1.7–3.6 °C~~ (MARGO Project Members, 2009; Tierney et al., 2020; Paul et al., 2021; Annan et al., 2022), whereas the SST difference in our experiment ~~was is~~ only 1.6 °C. A small difference in SST leads 265 to a small difference in CO₂ solubility between the two periods, ~~resulting in which causes~~ underestimation of the ~~amplitude of the magnitude of~~ atmospheric $p\text{CO}_2$. ~~Another possible reason is that the~~ Furthermore, it is important to note that this study did not consider specific processes that might have contributed to the ~~lower reduction in~~ atmospheric $p\text{CO}_2$ ~~introduced in Kobayashi et al. (2021), i.e., during the LGM, such as~~ enhanced salinity stratification, iron fertilization from glaciogenic dust, and carbonate compensation, ~~were not considered in this study.~~ as discussed in Kobayashi et al. (2021).

270 The differences in the steady-state ocean carbon cycles at 21 and 11 ~~kaBP~~ ka BP highlight the difficulty in accurately reproducing the actual changes in atmospheric $p\text{CO}_2$ in the transient experiment connecting these periods. Therefore, our analysis focuses on investigation of the impacts of climate change, particularly the notable variations in the AMOC, on the ocean carbon cycle, and reveals ~~model the~~ successes and deficiencies of the model through model–data comparison of carbon isotope signatures.

275 3.2 ~~Basin-scale Carbon isotope~~ changes ~~in carbon isotopes~~ during the last deglaciation

3.2.1 Radiocarbon isotopes

Here, we present the calculated transient changes in the ocean carbon cycle during the last deglaciation. During the deglaciation, atmospheric $\Delta^{14}\text{C}$ ~~was reported to decrease~~ decreases from approximately 500‰ to 0‰ (Fig. 2a). Seawater $\Delta\Delta^{14}\text{C}$ generally increases from ~~a the~~ relatively low LGM ~~value, although it might decrease at times (Figs~~ values, but decreases during HS1 and 280 the YD period (Fig. 2b–e). Generally, the state of the AMOC strongly influences the distribution of $\Delta\Delta^{14}\text{C}$. Both the model and the sediment core records show ~~an~~ increase in $\Delta\Delta^{14}\text{C}$ in the deep ocean during periods when the AMOC is relatively strong, e.g., the ~~Bølling–Allerød (BA) and Holocene, BA period and the Holocene (Fig. 3d and a-3f), and present~~ decrease in $\Delta\Delta^{14}\text{C}$ during periods when the AMOC is relatively weak, e.g., ~~Heinrich Stadial 1 (HS1) and the Younger Dryas (YD)~~. During the BA and Holocene, the zonal mean of $\Delta\Delta^{14}\text{C}$ remains above $-200‰$ throughout the Atlantic owing to active 285 ~~ventilation (Figs. 3d and f). Conversely, when the AMOC is relatively weak, the zonal mean of $\Delta\Delta^{14}\text{C}$ decreases to values below $-200‰$ in the deep ocean and the Southern Ocean, particularly during HS1 (Figs and the YD period (Fig. 3b and e-3c).~~ ventilation (Figs. 3d and f). Conversely, when the AMOC is relatively weak, the zonal mean of $\Delta\Delta^{14}\text{C}$ decreases to values below $-200‰$ in the deep ocean and the Southern Ocean, particularly during HS1 (Figs and the YD period (Fig. 3b and e-3c). The ~~pattern of calculated~~ changes in $\Delta\Delta^{14}\text{C}$ ~~induced by the changes in the AMOC is are~~ consistent with the pattern ~~seen observed~~ in the sediment core ~~records~~ record during a period characterized by rapid change in the AMOC after the BA transition (14.7 ka BP).

290 In the Pacific, when the AMOC is strong (i.e., at 13 and 11 kaBP), the $\Delta\Delta^{14}\text{C}$ in the South Pacific is relatively high, with elevated values from the surface to the deep Southern Ocean along the path of the AABW. ~~Some~~ The sediment core records compiled in Rafter et al. (2022) ~~indicate suggest~~ elevated $\Delta\Delta^{14}\text{C}$ ~~at depths near 1000 m values in the North Pacific intermediate layers~~ during HS1, possibly indicating the influence of the NPIW intrusion. However, the model results do not provide clear indication of the intrusion of young water masses (Figs. 3 and S4).

295 The compiled sediment core records ~~demonstrate substantial increase globally~~ globally show substantial increase in $\Delta\Delta^{14}\text{C}$ during HS1, ~~whereas~~. In contrast, the model experiment does not show such pronounced change (Figs Fig. 2b–e). This discrepancy can be attributed to ~~the fact that two main factors: failure of the model experiment did not accurately simulate the variations in ocean carbon storage, as reflected in the atmospheric $p\text{CO}_2$ to simulate activation of ocean ventilation during HS1, and the greater magnitude of the initial $\Delta\Delta^{14}\text{C}$ values at 21 ka BP relative to the reconstructed values. This is supported~~ by the insufficient carbon sequestration in the ocean calculated during the LGM (Fig. 2k). In other words, considering the glacial–interglacial redistribution of carbon in the atmosphere–ocean system, the relative ~~abundanees~~ abundance of ^{14}C to ^{12}C in the atmosphere ~~are is~~ higher during the ice age, as manifested in the atmospheric $\Delta^{14}\text{C}$ – CO_2 (Fig. 2a), ~~but~~; however, the variation in ^{12}C is not well reproduced in the model experiment (Fig. 2k).

The Regarding the latter point of insufficient carbon sequestration during the LGM, the triangles shown in Fig. 2 represent 305 the results of the best LGM simulation (LGM_all) conducted by Kobayashi et al. (2021). That simulation incorporated enhanced salinity stratification and sedimentation processes, which further contribute to accurate reproduction of low $\Delta\Delta^{14}\text{C}$ of deep water during the LGM. As shown in Figs Fig. 2b–e, there is substantial discrepancy between the model and the reconstruction, particularly in relation to the Southern Ocean during the period of early deglaciation. ~~The incorporation of changes~~ Incorporation of change in vertical mixing ~~, resulting from variations~~ resulting from variation in ocean stratification ~~, could~~ 310 potentially improve the $\Delta^{14}\text{C}$ simulation during simulation of $\Delta^{14}\text{C}$ in the deglaciation.

3.2.2 Stable carbon isotopes

Next, we focus on the changes in $\delta^{13}\text{C}$. For seawater $\delta^{13}\text{C}$, the overall trends of change ~~for in~~ $\delta^{13}\text{C}$ and $\Delta\Delta^{14}\text{C}$ are similar and correspond to phases of ~~climate climatic~~ change; however, $\delta^{13}\text{C}$ is less sensitive than $\Delta\Delta^{14}\text{C}$ to climate change (Fig. 2). This ~~could be associated with biological fractionation~~. ~~With a stronger AMOC, more light carbon is transported to~~ differential 315 response might be related to biological fractionation of carbon isotopes. A more active AMOC leads to increased biological activity that reduces $\delta^{13}\text{C}$ in deeper layers, especially in the North Atlantic, ~~due to increased biological production~~. This counteracts the effect influence of lighter carbon being transported to the surface by the active AMOC.

During HS1, ~~the AABW extends from the Southern Ocean into the deep ocean with relatively~~ $\delta^{13}\text{C}$ decreases gradually in the upper 3000 m of the North Atlantic (Figs. 2h, 4, and S3). The reduction in $\delta^{13}\text{C}$ can be attributed to several factors 320 (Gu et al., 2021) that include increased contribution from southern-sourced deep water with low $\delta^{13}\text{C}$ endmembers compared to the, accumulation of remineralized carbon with low $\delta^{13}\text{C}$ attributable to a weakened AMOC and reduced ventilation, and potential increase in the $\delta^{13}\text{C}$ endmember of North Atlantic Deep Water (NADW), leading to reduction. The results of this study show no clear change in the NADW endmembers of $\delta^{13}\text{C}$ (Fig. S5). Therefore, the change in $\delta^{13}\text{C}$ at approximately

3000 m is attributed to weakened ventilation in the North Atlantic, consistent with the reconstructed data (Fig. 2h). The data clearly show an increase in $\delta^{13}\text{C}$ in and to expansion of southern-sourced deep water. However, the mid-deep Southern Ocean (Figs. 2i and 4a–c). This change suggests loss of light carbon accumulated via biological processes during observed $\delta^{13}\text{C}$ change is relatively small compared to that derived from sediment core data because the AMOC change is less pronounced than that expected from the $^{231}\text{Pa}/^{230}\text{Th}$ reconstruction (McManus et al., 2004; Ng et al., 2018).

The deep Southern Ocean has its lowest $\delta^{13}\text{C}$ during the LGM, although the value gradually increases during HS1; however, this trend was not quantitatively simulated in the model. However, these observed changes are not reproduced in the model. According to Kobayashi et al. (2021), the low $\delta^{13}\text{C}$ during the LGM is related to enhanced Southern Ocean stratification and iron fertilization from glaciogenic dust. These processes, which are not considered in this study, contribute to the differences between the model and the observed data.

During the BA period (Fig. 4d) and the Holocene (Fig. 4f), when the AMOC is intensified, the intensified and deepened AMOC contributes to high $\delta^{13}\text{C}$ values originating from the North Atlantic Ocean expands into the deep ocean at penetrating to depths below 2000 m. The reconstructed basin-averaged $\delta^{13}\text{C}$ also shows reconstructions also show this increase in $\delta^{13}\text{C}$ in the deep ocean during the BA (Figs. especially in the Atlantic (Fig. 2g–j)). However, the data in contrast to the calculated change, the sediment core records do not show further reduction in $\delta^{13}\text{C}$ in the deep ocean during the YD, which is different from the calculated change period.

Changes in $\delta^{13}\text{C}$ in these deeper layers are also reflected the deep ocean lead to changes in atmospheric $\delta^{13}\text{C}\text{-CO}_2$. Atmospheric $\delta^{13}\text{C}\text{-CO}_2$ has a sharp drop in atmospheric $\delta^{13}\text{C}\text{-CO}_2$ during HS1, it then rises slightly followed by slight rise during the BA, before falling again period and then further decline during the YD, whereas period. However, the model-calculated changes in the ocean carbon cycle do not reproduce such a trend in atmospheric $\delta^{13}\text{C}\text{-CO}_2$ (Fig. 2f). The discrepancy between the model and data may be due to the contribution of vegetation. This will be discussed later reconstructed $\delta^{13}\text{C}\text{-CO}_2$ increases during the BA period, decreases during the YD period, and then increases again, whereas the model-calculated trend is the opposite. The discrepancy might involve the contribution from changes in vegetation, which is a topic discussed in Section 4.3.

In addition to changes in the deep ocean circulation, isotope fractionation by Isotope fractionation through temperature-dependent gas exchange and by phytoplankton, which preferentially takes up lighter carbon, is also an important factor for phytoplankton preference for uptake of lighter carbon also play important roles in $\delta^{13}\text{C}$ variation. Figure S6 shows the calculated changes in organic carbon export from that in 21 kaBP to ka BP with qualitative changes in biological flux reconstructed from proxies, specifically opal flux and alkenone flux, in sediment core records (Chase et al., 2003; Anderson et al., 2009; Bolton et al., 2011; Kohfeld and Chase, 2011; Martínez-García et al., 2014; Maier et al., 2015; Studer et al., 2015; Thiagarajan and McManus, 2019; Ai et al., 2020; Weber, 2021; Li et al., 2022). During HS1, both the models and the proxies show increased biological carbon transport in the Southern Hemisphere polar regions (Figs. polar region of the Southern Hemisphere (Fig. S6a–d)). In the polar regions, sea ice is reduced owing to warming, which could result in less light limitation and allow increased biological productivity. During HS1, however, biological carbon transport is reduced in the subpolar region and in the South Pacific gyres. These changes in the southern regions can be attributed to reduced nutrient supply

resulting from weakening of the AMOC. Another important factor is the ~~increased-increase in~~ iron limitation associated with
360 the reduced supply of dust-derived iron that affects biological production. During the BA warm period, the enhanced AMOC
enhances nutrient transport from the deep to the surface ocean, resulting in increased biological transport in the North Atlantic
(~~FigsFig. S6e and f6f~~). These changes in ~~the vertical~~ nutrient transport then propagate to the North Pacific. From the BA ~~to~~
~~YD period to the YD period~~, there is ~~an-increase in biological exports-export~~ in the Southern Ocean ~~,-which-may-be-attributed~~
~~to-a-that-might-be-attributable-to~~ reduction in sea ice ~~as-a-result-of-resulting from~~ warming in the Southern Hemisphere. The
365 factors that alter biological production in the model are understood ~~,-but need to be constrained from-using~~ additional proxy
data with high temporal resolution that can capture ~~of-millennial-scale variationvariations~~.

3.3 ~~Changes-Deglacial changes~~ in atmospheric $p\text{CO}_2$ ~~during the last deglaciation~~ caused by changes in the ocean carbon cycle

Figure 2k shows the calculated changes in atmospheric $p\text{CO}_2$ driven by ~~climate-and-carbon-cycle-changes-variations in the~~
370 ~~climate and the carbon cycle~~ during the last deglaciation. To investigate ~~those-the~~ factors driving the change in atmospheric
 $p\text{CO}_2$, we decomposed the factors relevant to the partial pressure of CO_2 at the sea surface ($p\text{CO}_2^{\text{os}}$). This parameter controls
atmospheric $p\text{CO}_2$ through gas exchange between the atmosphere and the ocean. Oceanic $p\text{CO}_2$ is ~~influneced-affected~~ by
temperature, salinity, DIC, and alkalinity, ~~which-are-factors-related-through-the-carbonate-system-The-impact-and-the-influence~~
of those factors on $p\text{CO}_2^{\text{os}}$ can be represented as follows:

$$p\text{CO}_2^{\text{os}} = f(\text{sDIC}, \text{sALK}, \text{SST}, \text{SSS}) \quad (1)$$

375 where sDIC is sea surface DIC, sALK is sea surface alkalinity, SST is sea surface temperature, and SSS is sea surface salinity.
The function f is determined based on the inorganic chemistry of the carbonate system (Millero, 1995). ~~By-analyzing-the~~
~~changes-in-each-variable-from-their-original-values,-we-can-determine-We-can-assess~~ the contribution of each ~~factor-to-the~~
~~variation-variable-to-the-changes~~ in $p\text{CO}_2^{\text{os}}$ ~~by-examining-the-change-in-each-variable-from-its-original-value~~.

3.3.1 Heinrich Stadial 1

380 During HS1, ~~the-calculated~~ atmospheric $p\text{CO}_2$ ~~rose-slightly-to-rises slightly until~~ approximately 17 ~~kaBP, then-rose-ka BP, and~~
~~then it rises~~ sharply to approximately 15 ~~kaBPka BP~~. From 18 to 15 ~~kaBPka BP~~, atmospheric $p\text{CO}_2$ ~~increased-increases~~ by
10.2 ppm (Fig. 5a), whereas the WAIS Divide ice core record shows ~~an-increase of 41.4 ppm during the same period~~ (Bauska
et al., 2021). The model ~~accounted-accounts~~ for approximately one quarter of the reconstructed changes in atmospheric $p\text{CO}_2$.
Decomposition analysis of $p\text{CO}_2^{\text{os}}$ ~~revealed-reveals~~ that most of the variation in $p\text{CO}_2^{\text{os}}$ is driven by ~~changes-change~~ in SST
385 (~~FigsFig. 5a and b~~). ~~Figures-S7b-and-e-show-the-5b~~. The changes in $p\text{CO}_2^{\text{os}}$ ($\Delta p\text{CO}_2^{\text{os}}$) attributable solely to variations
in ~~both-temperature and salinity~~ ($\Delta p\text{CO}_2^{\text{os}}(\text{TS})$) and ~~in~~ DIC and alkalinity ($\Delta p\text{CO}_2^{\text{os}}(\text{CA})$) ~~are shown in Fig. 6a and 6b,~~
~~respectively~~. It is evident that $\Delta p\text{CO}_2^{\text{os}}(\text{TS})$ shows a predominantly positive contribution globally, reflecting the pattern of
SST increase (Fig. ~~S7d6d~~), because increasing SST reduces CO_2 solubility. In other words, the main contributor to the ~~$p\text{CO}_2^{\text{os}}$~~
~~increase-increase in $p\text{CO}_2^{\text{os}}$~~ during HS1 is warming, especially in the subantarctic region.

390 3.3.2 Bølling-Allerød period

At the onset of the BA transition near 14.7 ~~kaBP~~ka BP, atmospheric $p\text{CO}_2$ ~~began~~begins to decrease, and this reduction ~~continued~~continues until 12.8 ~~kaBP~~ka BP (Fig. 2k). From 15 to 13 ka BP, atmospheric $p\text{CO}_2$ decreases by 7.0 ppm (Fig. 5c). During the BA period, the contributions of thermal changes and ~~geochemical changes acted~~biogeochemical changes act in opposition to the change in atmospheric $p\text{CO}_2$ (~~Figs~~Fig. 5c and d~~5d~~). At the onset of the BA period, as the AMOC ~~strengthened~~strengthens (Fig. 1a), SST and SSS both ~~increased~~increase in the Northern Hemisphere and ~~decreased~~decrease in the Southern Hemisphere (Fig. ~~S8d~~7d). The net contribution of $p\text{CO}_2^{\text{os}}$ (TS) attributable to changes in CO_2 solubility ~~was positive~~ (~~Figs~~is positive (Fig. 5c and d).~~On the other hand~~5d). ~~However~~, the enhanced AMOC facilitates the transport of nutrients, carbon, and alkalinity from the deep to the surface ocean, especially in the North Atlantic (~~Figs. S8e and f~~Fig. 7e and 7f). The increase in sDIC leads to ~~an~~increase in $p\text{CO}_2^{\text{os}}$, while the increase in sALK leads to ~~a~~reduction in $p\text{CO}_2^{\text{os}}$. These opposing effects ~~partially offset each other, resulting in net reduction in $p\text{CO}_2^{\text{os}}$ (Figs. 5c, 5d, and S8e).~~Additionally, as the AMOC resumed over time7c). During the AMOC overshoot at the BA transition and the subsequent stabilized phase, increased biological production in most of the global ocean ~~led to a~~contributes to millennial-scale decrease in sDIC, ~~contributing to decrease resulting in reduction~~ in $p\text{CO}_2^{\text{os}}$ (~~Figs~~Fig. 5c and d~~5d~~). In summary, following the recovery of the AMOC, the opposing contributions of $\Delta p\text{CO}_2^{\text{os}}$ (TS) and $\Delta p\text{CO}_2^{\text{os}}$ (CA) to $\Delta p\text{CO}_2^{\text{os}}$ over time ~~controlled~~control the temporal changes in $p\text{CO}_2^{\text{os}}$ and subsequent reduction in atmospheric $p\text{CO}_2$.

3.3.3 Younger Dryas period

Atmospheric $p\text{CO}_2$ ~~rose~~rises again at the onset of the YD period (12.8 ~~kaBP~~ka BP), coinciding with the collapse of the AMOC into a weak state (Fig. 1a). From 13 to 12 ka BP, atmospheric $p\text{CO}_2$ increases by 6.8 ppm (Fig. 5e). Decomposition analysis of $p\text{CO}_2^{\text{os}}$ ~~revealed~~reveals that the influences of $\Delta p\text{CO}_2^{\text{os}}$ (TS) and $\Delta p\text{CO}_2^{\text{os}}$ (CA) on the overall $\Delta p\text{CO}_2^{\text{os}}$ ~~were~~ in opposite directions. This are in opposition, and this offset is also observed during the BA period, but in the opposite sense. The contribution of $\Delta p\text{CO}_2^{\text{os}}$ (TS) ~~increased~~increases over time, leading to ~~an~~increase in $p\text{CO}_2^{\text{os}}$ (~~Figs~~Fig. 5e and f~~5f~~). The contribution of $\Delta p\text{CO}_2^{\text{os}}$ (CA) ~~was~~is small. As the AMOC ~~weakened~~weakens, reduction in sALK ~~contributed to an~~contributes to increase in $p\text{CO}_2^{\text{os}}$, but the decrease in sDIC ~~contributed to a~~contributes to reduction in $p\text{CO}_2^{\text{os}}$ (Figs. ~~5e and f, and S9e, e, and f).~~5f, 8c, 8e, and 8f); consequently, $p\text{CO}_2^{\text{os}}$ decreaseddecreases slightly during the YD period.

415 4 Discussion

~~This study investigated~~The objective of this study was to investigate the transient response of the ocean carbon cycle during the last deglaciation. By comparing the calculated carbon isotope signatures of $\delta^{13}\text{C}$ and $\Delta^{14}\text{C}$ with those ~~of~~derived from sediment core records, we can ~~identify potential biases and errors in the model, as well as examine~~assess the impacts of ~~climate and AMOC changes~~changes in climate and the AMOC on those signatures. ~~The simulation of carbon isotope signatures in addition to~~This comparison can also present information to help identify potential biases or missing processes within the model. In

addition to changes in atmospheric $p\text{CO}_2$ contributes to a comprehensive understanding of past the temporal changes in the global carbon cycle.

4.1 Response of carbon isotope signatures to drastic changes in the deep ocean circulation

425 Comparing the changes in $\Delta\Delta^{14}\text{C}$ variations between models and data allows us to evaluate the accuracy of the computed AMOC variations. The reconstructed $\Delta\Delta^{14}\text{C}$ rises notably during HS1, in contrast to the less pronounced shift seen in the model experiment (Fig. 2b–e). Two primary factors contribute to this discrepancy: underestimation of the activation of ocean ventilation during HS1 by the model, and the higher calculated $\Delta\Delta^{14}\text{C}$ values relative to the reconstructed low values of $\Delta\Delta^{14}\text{C}$ in the deep ocean during the LGM. The difficulty in reproducing changes in $\Delta\Delta^{14}\text{C}$ might also be related to underestimation of variations in atmospheric $p\text{CO}_2$ during this
430 period. Processes that might contribute to this problem are discussed in more detail in Section 4.2.

After the BA transition, the variations in $\Delta\Delta^{14}\text{C}$ regarding the notable shifts in the AMOC after the BA transition are generally consistent with those of the reconstruction. Corresponding to the AMOC change, $\Delta\Delta^{14}\text{C}$ increases in the deep ocean from the deep Atlantic to the Pacific Ocean (Figs. 2e–eFig. 2c–e). Subsequently, $\Delta\Delta^{14}\text{C}$ decreased from the Atlantic Ocean to the Southern Ocean during the YD period in response to the weakening of the AMOC.
435 This change is consistent with the reconstruction, but there is overestimation of the quantitative changes in the deep ocean are overestimated (Fig. 3e). This may that could be related to the reproducibility of the ocean circulation fields, which will be is a topic that is discussed below.

Pöppelmeier et al. (2023) use Bern3D model to estimate the AMOC changes during the last deglaciation from by Pöppelmeier et al. (2023) involved conducting transient model simulations using the Bern3D model. They performed
440 multiple model–data comparisons between including carbon isotope ratios, ϵNd , and $^{231}\text{Pa}/^{230}\text{Th}$. Their research suggests that the AMOC gradually weakens results suggest gradual weakening of the AMOC during HS1, recovers recovery at the BA transition, and weakens again subsequent weakening during the YD, but it does not completely collapse. This period, albeit without a complete collapse. The proposed pattern of AMOC change is qualitatively consistent with our the ocean modeling of Obase and Abe-Ouchi (2019) (Fig. 1a). The Bern3D study also shows indicates that the proportion of deep water originating
445 from the North Atlantic is not much different from during the YD period is little different to that during the BA because of the short duration of the YD period. In contrast Conversely, this study shows that drastic changes in the distribution of $\Delta^{14}\text{C}$ and $\delta^{13}\text{C}$ changes almost completely at the basin scale in response to changes in the AMOC over approximately 1000 years AMOC variations over a span of approximately 1000 years (Figs. 3 and 4). Our model indicates a longer period of shows longer duration of the relatively weak AMOC during the YD compared to period compared to that in the Bern3D model, which
450 helps to explain the discrepancies. The AMOC remains relatively weak for 1000 years, with a maximum volume transport of approximately 4 Sv. However, the Bern3D model shows a minimum volume transport of the AMOC of approximately 6 Sv during the YD period, which gradually increases to nearly 9 Sv during the following millennium. These differences are partly attributable to variation in the freshwater input to the North Atlantic between the two models. The stagnation of the AMOC in our model provides an explanation for the differences observed between the model and data in the data in relation

455 to the deep North Atlantic during the YD period. However, it is ~~important~~ critical to recognize that ~~even with similarities in AMOC strength changes, there are differences in the overall~~ despite similarities in the fluctuations of the strength of the AMOC, differences remain among models in terms of the broader deep ocean circulation ~~field~~ patterns, including the AABW ; ~~between models, resulting in differences in basin-scale chemical tracer changes. Since each model has and~~ Pacific meridional overturning. Consequently, these differences result in different chemical tracer distributions at the basin scale. Considering
460 ~~that each model contains~~ systematic biases in both physical and biogeochemical processes, ~~it is valuable to compare multiple models to explore realistic AMOC variations in the past. The importance of this study is that it examines how the AMOC mode change affects the three-dimensional structure of water masses, not only in the Atlantic, but also in the Southern and Pacific oceans.~~ comparative analysis of multiple models becomes invaluable for exploring past AMOC variations.

Further information can be obtained by comparing the results of model–data comparisons for $\Delta\Delta^{14}\text{C}$ and $\delta^{13}\text{C}$. For $\delta^{13}\text{C}$,
465 ~~both the model and data show the same trend of an~~ the data show similar trends, depicting increase in deep water $\delta^{13}\text{C}$ during the BA ~~as~~ period as in $\Delta\Delta^{14}\text{C}$. ~~After that, the model shows a decrease~~ However, there is a discrepancy during the subsequent
~~YD period, whereas this feature is absent in the reconstruction (Fig. 2g–j). The mismatch is particularly pronounced from the Southern Ocean to the deep ocean. Possible contributing factors include variations in the signal of change~~ There are several
470 ~~possible factors that could potentially influence this discrepancy. For example, variations in change signals and potential dating inaccuracies within individual sediment core data could result from smoothing effects such as bioturbation and coring artifacts. These complexities highlight the need for caution when comparing model simulations and sediment core records. Another important factor is the weakening of the simulated AMOC during the YD period. Comparison of the model and sediment data for $\Delta\Delta^{14}\text{C}$ and dating errors in individual sediment data. Another factor is that not only ocean circulation but also ecosystem responses are not adequately reproduced. The calculated $\delta^{13}\text{C}$ suggests that the weakening of the AMOC during the YD period might be overly pronounced in the model (Figs. 3e and 4e). Additionally, the calculated increase in export of biogenic organic matter in the Southern Ocean increased during the YD period compared to that in the BA period (Figs. S6f and g), resulting in a decrease in $\delta^{13}\text{C}$ from the Southern Ocean to the deep ocean. This biological response demonstrates that, without this change, a~~ S6g) contributes to the decrease in $\delta^{13}\text{C}$ ~~would not be observed in the deep ocean. Since a decrease in nutrient concentrations limits biological productivity, it is crucial to accurately simulate the~~ This emphasizes the importance of accurately simulating nutrient and iron cycles ~~associated with nutrient limitation of biological productivity. In particular, as, especially in iron-limited regions affected by changes in dust-derived iron supply. As the Southern Hemisphere warms and becomes more humid, the supply of iron from dust may might decrease (Martin, 1990; Martínez-García et al., 2014). This change has a substantial impact on ocean productivity in iron-limited regions, which subsequently affects atmospheric $p\text{CO}_2$. The interpretation of discrepancies between models and data on~~ Reproducing changes in $\delta^{13}\text{C}$ is challenging owing to the intricate interconnections between ocean circulation, biological processes, and atmosphere–ocean gas exchange. Understanding the discrepancies between the model and the data in terms of the $\delta^{13}\text{C}$ changes is an open question will require future sensitivity experiments to clarify their respective contributions and to provide deeper understanding of these factors.

4.2 Insights from carbon isotope ratios: oceanic CO₂ release ~~from the ocean to~~ during the atmosphere ~~deglaciation~~

490 Ocean modeling with freshwater forcing experiments has provided insight ~~insights~~ into the link between the shutdown and resumption of the AMOC and the changes in atmospheric $p\text{CO}_2$. Schmittner and Galbraith (2008) ~~showed~~ demonstrated that cessation of the AMOC ~~leads to an~~ causes increase in atmospheric $p\text{CO}_2$ ~~, which is due owing~~ to several factors. ~~The First, the efficiency of the biological carbon pumps in NADW pump in the North Atlantic is relatively high compared with that in AABW, and therefore the reduced inflow of NADW leads to reduction to that in the Southern Ocean. Therefore, reduction~~
495 in the NADW inflow leads to decrease in biological carbon sequestration in the deep ocean. ~~Moreover~~ Second, weakening of ~~the~~ Southern Ocean stratification ~~, associated with AMOC shutdown, , associated with shutdown of the AMOC~~ increases the outgassing of CO₂ from the ocean to the atmosphere. ~~This study confirms-~~

The results of this study confirm the gradual increase in atmospheric $p\text{CO}_2$ during HS1 and ~~YD~~ the YD period in parallel with the ~~AMOC weakening, but~~ weakened state of the AMOC; however, such an increase is not directly related to a reduction
500 in the regenerated nutrient inventory, as suggested by Schmittner and Galbraith (2008). The reason for this difference is that the contribution of the change in changes in temperature and alkalinity to the change in $p\text{CO}_2^{\text{os}}$ during the YD ~~was~~ period is greater than the contribution of the change in DIC in this study. When the AMOC changes, the ~~resulting atmospheric $p\text{CO}_2$ anomaly depends non-thermal effects on changes in $p\text{CO}_2^{\text{os}}$ mainly depend~~ on the magnitude of the relative contributions of DIC and alkalinity to $p\text{CO}_2^{\text{os}}$, based on the vertical gradient of DIC and alkalinity between the surface and the deeper ocean.
505 ~~While the $p\text{CO}_2$ response varies depending on the model used and the initial distribution of DIC and alkalinity, this study shows that increased SST and reduced surface ocean alkalinity emerge as major contributors to the deglacial increase in-~~

Although our results show the impact of drastic changes in the AMOC on atmospheric $p\text{CO}_2$ ~~-~~
Simulating changes in $\Delta\Delta^{14}\text{C}$ during the early deglaciation is challenging. During HS1, the sediment core records show that $\Delta\Delta^{14}\text{C}$ increased by 200‰ in the deep Southern Ocean and by 100‰ in other deep oceans (Figs. 2c–e). The idea that
510 ventilation increased during HS1 and that CO₂ was released from the oceans into the atmosphere is consistent with the increase during the last deglaciation, the model does not fully explain the variations in atmospheric $p\text{CO}_2$ during ~~this period. In contrast, the current model cannot fully reproduce the large changes in ventilation. The process that may be involved in this change in ventilation during HS1 is discussed below.-~~

~~Ice core reconstructions show that~~ the early deglaciation. Ice core records indicate a rise of approximately 40 ppm in
515 atmospheric $p\text{CO}_2$ accompanied by reduction in atmospheric $\delta^{13}\text{C}\text{-CO}_2$ ~~is depleted during HS1, but the calculated $\delta^{13}\text{C}$ and $\Delta^{14}\text{C}\text{-CO}_2$ during HS1. However, the calculated~~ variations are insufficient in terms of ~~its~~ their amplitude (Fig. 2a, 2f). ~~One factor-, and 2k). A key contributor to this discrepancy is the limited amplitude of the ventilation change, as evidenced by the change in $\Delta\Delta^{14}\text{C}$, because the upwelling of light carbon to the upper layers and its exchange between the ocean and the atmosphere lead to a reduction in atmospheric $\delta^{13}\text{C}\text{-CO}_2$. In Kobayashi et al. (2021), extent of the change in ventilation,~~
520 evident from the $\Delta\Delta^{14}\text{C}$ changes in the ocean (Fig. 2b–e). However, the current model has difficulty fully reproducing these substantial changes in ventilation.

In addition to the changes in ventilation, biological processes are important in explaining the deglacial carbon cycle changes. Kobayashi et al. (2021) indicated that iron fertilization from glaciogenic dust ~~was shown to increase~~ increases biological production in the subantarctic region, ~~which contributed thereby contributing~~ to the reproduction of low $\delta^{13}\text{C}$ in the deep Southern Ocean during the LGM. ~~Their study does~~ However, their study did not reproduce the ~~extremely old water suggested by radiocarbon~~ profoundly old deep water in the deep glacial Southern Ocean, as suggested by radiocarbon data (triangles in Fig. 2d), but it ~~does reproduce~~ did reproduce the low $\delta^{13}\text{C}$ values (triangles in Fig. 2i). The change in glaciogenic dust deposition was not considered in this study, and therefore the model might underestimate the glacial-interglacial variation in biological production in the subantarctic region, ~~which might contribute to potentially contributing to the~~ underestimation of the changes in atmospheric and deep-sea $\delta^{13}\text{C}$ during HS1. ~~In future efforts to reproduce the carbon cycle during HS1, the model-data comparison of $\Delta\Delta^{14}\text{C}$ and $\delta^{13}\text{C}$ shows that it is important to reproduce both the activation of ventilation and the changes in biological production, including the strengthening of iron limitation in the Southern Ocean.~~

~~Besides, in the North Pacific, Moreover, while many studies focused primarily on environmental changes in the Atlantic, the contributions from other ocean basins are also important. For example, sediment core records show from the North Pacific~~ indicate increase in $\Delta\Delta^{14}\text{C}$ at depth near 1000 m during HS1 (Okazaki et al., 2010; Rae et al., 2014; Rafter et al., 2022). ~~The NPIW was suggested to be strengthened or deepened during HS1, but this change is only partially explained by the calculated changes in $\Delta\Delta^{14}\text{C}$. By analyzing Analysis of radiocarbon and boron isotopes in sediment cores ;Rae et al. (2014) show that the by Rae et al. (2014) revealed that the extent of the NPIW expanded during HS1. Using an EMIC of GENIE, they show that these ventilation changes contribute to an increase~~ These ventilation changes have potential to contribute to the rise in atmospheric $p\text{CO}_2$. Chikamoto et al. (2012) compared ~~an AOGCM of MIROC, the model we use, with an EMIC of LOVECLIM. They show that both models concur on the activation of the NPIW when freshwater flows~~ two coupled climate models, i.e., MIROC version 3.1 and LOVECLIM, and showed consistent results for activation of ventilation of NPIW triggered by freshwater inflow into the North Atlantic. ~~However, it is also indicated that the response of the ocean circulation is less pronounced in MIROC. The activation of the ocean circulation and the~~ The processes of activation of ocean ventilation and subsequent degassing of CO_2 in the North Pacific during the early deglaciation ~~are processes that have the potential to could~~ contribute to the currently unexplained increase in atmospheric $p\text{CO}_2$.

~~High-resolution~~ The high-resolution ice core data obtained from the WAIS Divide ~~provide record provides~~ valuable insights into the ~~changes in atmospheric $p\text{CO}_2$ time scale of the changes in the carbon cycle~~ during the last deglaciation. It is suggested that there are two modes of change in relation to atmospheric $p\text{CO}_2$: slow increase on the millennial scale and rapid increase on the centennial scale (Marcott et al., 2014). The rapid increase in atmospheric $p\text{CO}_2$ of 10–15 ppm at the end of HS1 (14.8 kaBP ka BP) and at the end of ~~YD~~ the YD period (11.7 kaBP ka BP) over a short period of 100–200 years ~~;is~~ is synchronized with the resumption of the AMOC (McManus et al., 2004; Ng et al., 2018). However, this study did not reproduce such abrupt changes in atmospheric $p\text{CO}_2$. Several factors might contribute to this discrepancy, including insufficient temperature rise in the Southern Hemisphere associated with ~~AMOC changes~~ change in the AMOC, inadequate representation of the vertical concentration gradients of DIC and alkalinity, limitations in capturing atmospheric and oceanic dynamics in the general circulation model, and the influence of small-scale phenomena. Previous modeling studies have suggested that deeper convection in the

Southern Ocean and a strengthening of westerly winds in the Southern Hemisphere could contribute to the abrupt jump in atmospheric $p\text{CO}_2$ during the middle of HS1 (16.3 kaBP) by transporting sequestered carbon from the deep Southern Ocean to the surface (Menviel et al., 2018). ~~Since these~~ These processes are related to the challenges in reproducing carbon isotope ratios described ~~earlier, these results suggest that~~ above; therefore, this discussion points to the necessity of improving our AOGCM and of refining its experimental setup ~~need to be improved in future studies, as previewed in Section 4.3.~~

4.3 ~~Implications for future improvements to~~ Improvement of the model and the experimental design: future implications

Model–data comparisons of carbon isotope signatures underscore the importance of refining our climate models to more accurately represent the complex interactions that govern changes in the carbon cycle. Future improvements to the AOGCM ~~may include~~ used in this study might address the following considerations.

~~For example~~ Currently, the AOGCM ~~used in this study did~~ does not account for temporal changes in ~~the ice sheet and underestimated the ice sheets and it underestimates the changes in~~ Southern Ocean SST ~~changes (Obase and Abe-Ouchi, 2019)~~ There (Obase and Abe-Ouchi, 2019). Moreover, there is some uncertainty ~~as to how much meltwater has flowed regarding~~ the volume of meltwater flow across the North Atlantic during HS1 (Ivanovic et al., 2018; Snoll et al., 2023) and ~~BA (Kapsch et al., 2022; Bouttes et al., 2023). This the BA period (Kapsch et al., 2022; Bouttes et al., 2023). It~~ suggests that the problem ~~persists within the AOGCM, where the model's is integral to the AOGCM because the~~ AMOC response is not consistently ~~realistically reproduced and realistically observed~~, even when realistic freshwater variations are applied. Furthermore, as ~~shown in~~ identified by Obase et al. (2023), the magnitude of ocean warming during the last deglaciation varies depending on the response characteristics of each model, resulting in a range across multiple models. Sherriff-Tadano et al. (2023) demonstrated that ~~altering~~ alteration of parameters associated with cloud thermodynamic phase fractions in a climate model ~~mitigates warming biases~~ reduces the warming bias of SST in the modern Southern Ocean. Using a model with a reduced Southern Ocean warming bias ~~is expected to yield, we expect to obtain~~ different responses in Southern Ocean SST and ocean circulation during the glacial period, ~~as well as and~~ in their changes during the deglaciation, compared to those derived in this study. ~~Furthermore, although some studies propose~~ Some studies proposed potential alterations in the westerly winds over the Southern Ocean throughout the last deglaciation (Gray et al., 2023), but there is a substantial degree of uncertainty concerning the anticipated changes in ~~atmospheric dynamics during the deglaciation. These the atmospheric dynamics. Those~~ uncertainties could have a substantial impact on the results of ocean biogeochemical ~~models~~ cycle modeling and, consequently, on atmospheric $p\text{CO}_2$. Efforts to ~~mitigate biases and facilitate a comprehensive discussion of climate model coherence~~ reduce bias and to facilitate comprehensive discussion regarding climate model consistency are critical to advancing future ~~climate-carbon~~ climate-carbon cycle modeling. These endeavors are essential to refine our understanding of the complex interactions between climate and the carbon cycle.

In addition to those factors mentioned above, there are several other factors that could contribute to improving the simulation of the ocean carbon cycle during the ~~period of the~~ last deglaciation. One important consideration is the inclusion of critical processes for ~~lowing~~ lowering atmospheric $p\text{CO}_2$ during the LGM, which ~~were~~ are identified in Kobayashi et al. (2021).

Those processes include enhanced stratification of the Southern Ocean, iron fertilization from glaciogenic dust, and carbonate compensation. Understanding the changes in those processes during the deglaciation is critical, and ~~properly incorporating them~~ their proper incorporation into future modeling efforts might lead to both improved simulations and better understanding of the dynamics during this period. ~~In addition, it has been reported that the inclusion of a~~ Studies have also reported that inclusion of ~~the~~ parameterization of vertical mixing ~~that depends on the~~, which depends on tidal mixing energy and stratification ~~can~~, could help better reproduce the ~~Pacific circulation deep ocean circulation in the Pacific~~ (Oka and Niwa, 2013; Kawasaki et al., 2022). The introduction of tidal mixing parameterization has also proven effective in reproducing $\delta^{13}\text{C}$ and $\Delta^{14}\text{C}$ in the glacial ocean (Wilmes et al., 2021). Incorporating the insights from these model ~~development~~ developments has the potential to lead to a more realistic representation of carbon cycle variations during the glacial period and subsequent deglaciation.

~~Furthermore~~ Moreover, glacial–interglacial changes in ocean volume due to ice sheet changes also have an impact on the carbon cycle. A recent study analyzing PMIP model outputs highlighted the importance of accurate representation of ocean volume changes and their associated effects on alkalinity adjustments (Lhardy et al., 2021). For more accurate simulations, it is critical to perform numerical integration that accounts for temporal changes in ocean volume during the deglaciation.

It is also worth noting that carbon exchange between the atmosphere and the ocean is not the sole driver of deglacial variation in atmospheric $p\text{CO}_2$. Changes in terrestrial and soil carbon storage also play important roles in modulating atmospheric $\delta^{13}\text{C}$ ~~and $p\text{CO}_2$ during the deglaciation (Schmitt et al., 2012; Bauska et al., 2021). Trends in atmospheric $\delta^{13}\text{C}$ - CO_2 changes differ between the reconstruction and the model (Fig. 2f). The model shows that, contrary to the reconstruction, atmospheric $\delta^{13}\text{C}$ - CO_2 decreases during the BA and increases during the YD. A possible explanatory factor, in addition to the challenges of reproducing biological productivity mentioned above, is that there is a lack of preferential uptake of light carbon by terrestrial~~ vegetation and $p\text{CO}_2$ during the last deglaciation (Schmitt et al., 2012; Jeltsch-Thömmes et al., 2019; Bauska et al., 2021). Comparison of $\Delta^{14}\text{C}$ - CO_2 and $\delta^{13}\text{C}$ - CO_2 provides a consistent explanation if carbon uptake by vegetation expands during the BA period and declines during the YD period, as suggested by Schmitt et al. (2012). Vegetation growth, driven prompted by CO_2 fertilization, can act as a sink for CO_2 and counteract the rise carbon sink, offsetting the increase in atmospheric $p\text{CO}_2$ (Bouttes et al., 2012a; Menviel et al., 2012). Therefore, it may be possible to revisit the changes in atmospheric $p\text{CO}_2$ during the BA and YD periods that were described by the ocean-only processes in this study

In this study, we applied the same sea surface restoring terms for the carbon isotopes used during the initial spin-up of the LGM throughout the deglaciation experiment. In other words, this approach did not consider changes in vegetation or changes in ^{14}C production in the atmosphere. Future studies using Earth system models that include both terrestrial and oceanic carbon cycle processes would contribute to more enhance our comprehensive understanding of glacial changes in carbon cycles. A study of the carbon cycle associated with the glacial Dansgaard–Oeschger events ~~has been conducted in an ESM of CESM1 and has shown that at this time scale,~~ conducted using an earth system model, revealed that the changes in terrestrial carbon storage at this time scale are as important as those in the oceans (Jochum et al., 2022). Moreover, in previous studies using EMICs Earth System Models of Intermediate Complexity, temporal variations in atmospheric $p\text{CO}_2$ are primarily used to calculate changes in radiative forcing, and several studies have explored the interaction between the carbon cycle and the climate (Bouttes et al., 2012a; Ganopolski and Brovkin,

625 2017). Although fully coupling a carbon cycle model ~~with to~~ a climate model is a more advanced endeavor, we are ~~interested~~
~~in pursuing such~~ eager to explore this avenue in future research.

5 Conclusions

To understand the mechanisms of glacial–interglacial variability in the carbon cycle, this study ~~focused on the last deglaciation~~
~~period and investigated~~ examined the transient response of the ocean carbon cycle to climate change, including the ~~significant~~
630 ~~remarkable~~ strengthening and weakening of the AMOC at the BA and YD transitions. This study represents an important step
toward comprehensive transient simulations of the carbon cycle using an AOGCM, even though the changes in atmospheric
 $p\text{CO}_2$ are relatively small compared to those derived from ice core reconstructions. The importance of this study lies in its
model–data comparisons of carbon isotope ratios that elucidate the impact of AMOC mode changes on the three-dimensional
structure of water masses in the Atlantic, Southern, and Pacific oceans.

635 Our model qualitatively simulates an increase in atmospheric $p\text{CO}_2$ during HS1. The calculated increase of approximately
10 ppm in atmospheric $p\text{CO}_2$ ~~increase was found to be caused by an~~ from 18 to 15 ka BP is mainly caused by increase
in SST. The relatively modest increase in atmospheric $p\text{CO}_2$, compared ~~with that of the ice core record~~ to that of ice core
records, might be attributable in part to relatively small increases in SST in the Southern Ocean. ~~Furthermore, model–data~~
~~comparisons~~ Additionally, comparison of carbon isotope signatures ~~suggest that the model inaccurately represents the~~ between
640 the model and the data highlighted the scope for improvement in the representation of increased ventilation in the deep ocean
and the ~~decreased efficiency of~~ North Pacific. Similarly, there is potential for improvement with respect to changes in surface
biological productivity ~~in the Southern Ocean and underestimates the activation of the NPIW. This, in turn, contributes to an~~
~~underestimation~~ involving the nutrient cycle, including iron. Correction of these elements would substantially improve our
understanding of the increase in atmospheric $p\text{CO}_2$ during the early deglaciation.

645 ~~During~~ The drastic shifts in the AMOC during the BA and YD periods, ~~large changes in the AMOC caused~~ cause bipolar
climate changes, ~~altering~~. These changes affect not only the ~~distributions of~~ temperature and salinity, ~~but also affecting~~
~~the vertical gradients~~ distributions but also the distributions of DIC and alkalinity. ~~The net effects of those~~ Interestingly, the
cumulative effects of these changes on atmospheric $p\text{CO}_2$ appear to ~~be mutually offsetting, with~~ cancel each other out, resulting
in only slight decrease during the BA period and increase during the YD. ~~It was found that not only the change in $p\text{CO}_2^{os}$~~
650 ~~due to changes in the amount of regenerated carbon accumulated by biological processes, but also the change in~~ period. It
is noticeable that changes in $p\text{CO}_2^{os}$ due to ~~changes in alkalinity contributed more significantly during the BA and lowering~~
~~variations in temperature and alkalinity play a major role in the reduction of~~ atmospheric $p\text{CO}_2$ during the BA period.

To simulate transient changes in the carbon cycle, ~~model biases, experimental settings~~ improvements in model accuracy,
experimental configurations, and the models themselves ~~need to be improved to more realistically capture~~ are critical for
655 capturing the dynamical and biogeochemical changes in the atmosphere and ocean. Further research is needed to ~~clarify what~~
~~processes contribute to~~ identify the specific processes that influence changes in the ocean carbon cycle ~~at over~~ different time
scales in ~~each ocean basin~~ individual ocean basins. We emphasize ~~that the analysis of the importance of analyzing~~ carbon

isotope variations ~~provides that can provide valuable~~ insights into past carbon cycle dynamics and ~~contributes to a better understanding of glacial-interglacial~~ contribute to comprehensive understanding of the glacial-interglacial variations in the
660 ocean carbon cycle.

Code and data availability. The CCSR Ocean Component Model (COCO) is the ocean general circulation model of MIROC, and the code of COCO version 4.0 is included as part of MIROC-ES2L. The source code of MIROC-ES2L can be obtained from <https://doi.org/10.5281/zenodo.3893386> (Ohgaito et al., 2021).

Author contributions. H.K. and A.O. designed the research. H.K. conducted the numerical experiments with help from T.O. H.K. performed
665 the analysis and wrote the paper. A.O. and A.A.O. obtained funding and supervised the study. All authors discussed the results and commented on the manuscript.

Competing interests. The authors declare that they have no competing interests.

Acknowledgements. The authors express sincere gratitude to the two anonymous reviewers for their invaluable and constructive feedback on our manuscript. This work was supported by JSPS KAKENHI Grant Numbers JP17H06104, JP17H06323, JP19H01963, and JP21K13990.
670 The ocean tracer model simulations in this study were performed at the Information Technology Center of the University of Tokyo. We thank James Buxton MSc, from Edanz (<https://jp.edanz.com/ac>), for editing a draft of this manuscript.

References

- Ai, X. E., Studer, A. S., Sigman, D. M., Martínez-García, A., Fripiat, F., Thöle, L. M., Michel, E., Gottschalk, J., Arnold, L., Moretti, S., Schmitt, M., Oleynik, S., Jaccard, S. L., and Haug, G. H.: Southern Ocean upwelling, Earth's obliquity, and glacial-interglacial atmospheric CO₂ change, *Science*, 370, 1348–1352, <https://doi.org/10.1126/science.abd2115>, 2020.
- Anderson, R. F., Ali, S., Bradtmiller, L. I., Nielsen, S. H. H., Fleisher, M. Q., Anderson, B. E., and Burckle, L. H.: Wind-Driven Upwelling in the Southern Ocean and the Deglacial Rise in Atmospheric CO₂, *Science*, 323, 1443–1448, <https://doi.org/10.1126/science.1167441>, 2009.
- Annan, J. D., Hargreaves, J. C., and Mauritsen, T.: A new global surface temperature reconstruction for the Last Glacial Maximum, *Climate of the Past*, 18, 1883–1896, <https://doi.org/10.5194/cp-18-1883-2022>, 2022.
- Barnola, J. M., Raynaud, D., Korotkevich, Y. S., and Lorius, C.: Vostok ice core provides 160, 000-year record of atmospheric CO₂, *Nature*, 329, 408–414, <https://doi.org/10.1038/329408a0>, 1987.
- Bauska, T. K., Marcott, S. A., and Brook, E. J.: Abrupt changes in the global carbon cycle during the last glacial period, *Nature Geoscience*, 14, 91–96, <https://doi.org/10.1038/s41561-020-00680-2>, 2021.
- Bereiter, B., Eggleston, S., Schmitt, J., Nehrbass-Ahles, C., Stocker, T. F., Fischer, H., Kipfstuhl, S., and Chappellaz, J.: Revision of the EPICA Dome C CO₂ record from 800 to 600 kyr before present, *Geophysical Research Letters*, 42, 542–549, <https://doi.org/10.1002/2014gl061957>, 2015.
- Bereiter, B., Shackleton, S., Baggenstos, D., Kawamura, K., and Severinghaus, J.: Mean global ocean temperatures during the last glacial transition, *Nature*, 553, 39744, <https://doi.org/10.1038/nature25152>, 2018.
- Bolton, C. T., Lawrence, K. T., Gibbs, S. J., Wilson, P. A., and Herbert, T. D.: Biotic and geochemical evidence for a global latitudinal shift in ocean biogeochemistry and export productivity during the late Pliocene, *Earth and Planetary Science Letters*, 308, 200–210, <https://doi.org/10.1016/j.epsl.2011.05.046>, 2011.
- Bouttes, N., Paillard, D., Roche, D. M., Waelbroeck, C., Kageyama, M., Laurantou, A., Michel, E., and Bopp, L.: Impact of oceanic processes on the carbon cycle during the last termination, *Climate of the Past*, 8, 149–170, <https://doi.org/10.5194/cp-8-149-2012>, 2012a.
- Bouttes, N., Roche, D. M., and Paillard, D.: Systematic study of the impact of fresh water fluxes on the glacial carbon cycle, *Climate of the Past*, 8, 589–607, <https://doi.org/10.5194/cp-8-589-2012>, 2012b.
- Bouttes, N., Lhardy, F., Quiquet, A., Paillard, D., Goosse, H., and Roche, D. M.: Deglacial climate changes as forced by different ice sheet reconstructions, *Climate of the Past*, 19, 1027–1042, <https://doi.org/10.5194/cp-19-1027-2023>, 2023.
- Broecker, W. S. and Maier-Reimer, E.: The influence of air and sea exchange on the carbon isotope distribution in the sea, *Global Biogeochemical Cycles*, 6, 315–320, <https://doi.org/10.1029/92gb01672>, 1992.
- Brovkin, V., Ganopolski, A., Archer, D., and Munhoven, G.: Glacial CO₂ cycle as a succession of key physical and biogeochemical processes, *Climate of the Past*, 8, 251–264, <https://doi.org/10.5194/cp-8-251-2012>, 2012.
- Chase, Z., Anderson, R. F., Fleisher, M. Q., and Kubik, P. W.: Accumulation of biogenic and lithogenic material in the Pacific sector of the Southern Ocean during the past 40, 000 years, *Deep Sea Research Part II: Topical Studies in Oceanography*, 50, 799–832, [https://doi.org/10.1016/s0967-0645\(02\)00595-7](https://doi.org/10.1016/s0967-0645(02)00595-7), 2003.
- Chikamoto, M. O., Menviel, L., Abe-Ouchi, A., Ohgaito, R., Timmermann, A., Okazaki, Y., Harada, N., Oka, A., and Mouchet, A.: Variability in North Pacific intermediate and deep water ventilation during Heinrich events in two coupled climate models, *Deep Sea Research Part II: Topical Studies in Oceanography*, 61-64, 114–126, <https://doi.org/10.1016/j.dsr2.2011.12.002>, 2012.

- Conkright, M. E., Garcia, H. E., O'Brien, T. D., Locarnini, R. A., Boyer, T. P., Stephens, C., and Antonov, J. I.: World Ocean Atlas 2001, vol. 4, Nutrients, NOAA Atlas NESDIS, vol. 52, p. 392 pp., NOAA, Silver Spring, Md., 2002.
- 710 Dome Fuji Ice Core Project Members: State dependence of climatic instability over the past 720,000 years from Antarctic ice cores and climate modeling, *Science Advances*, 3, e1600446, <https://doi.org/10.1126/sciadv.1600446>, 2017.
- Ganopolski, A. and Brovkin, V.: Simulation of climate, ice sheets and CO₂ evolution during the last four glacial cycles with an Earth system model of intermediate complexity, *Climate of the Past*, 13, 1695–1716, <https://doi.org/10.5194/cp-13-1695-2017>, 2017.
- 715 Ganopolski, A. and Roche, D. M.: On the nature of lead–lag relationships during glacial–interglacial climate transitions, *Quaternary Science Reviews*, 28, 3361–3378, <https://doi.org/10.1016/j.quascirev.2009.09.019>, 2009.
- Gottschalk, J., Battaglia, G., Fischer, H., Frölicher, T. L., Jaccard, S. L., Jeltsch-Thömmes, A., Joos, F., Köhler, P., Meissner, K. J., Menviel, L., Nehrbass-Ahles, C., Schmitt, J., Schmittner, A., Skinner, L. C., and Stocker, T. F.: Mechanisms of millennial-scale atmospheric CO₂ change in numerical model simulations, *Quaternary Science Reviews*, 220, 30–74, <https://doi.org/10.1016/j.quascirev.2019.05.013>, 2019.
- 720 Gray, W. R., de Lavergne, C., Wills, R. C. J., Menviel, L., Spence, P., Holzer, M., Kageyama, M., and Michel, E.: Poleward Shift in the Southern Hemisphere Westerly Winds Synchronous With the Deglacial Rise in CO₂, *Paleoceanography and Paleoclimatology*, 38, e2023PA004666, <https://doi.org/10.1029/2023pa004666>, 2023.
- Gu, S., Liu, Z., Oppo, D. W., Lynch-Stieglitz, J., Jahn, A., Zhang, J., Lindsay, K., and Wu, L.: Remineralization dominating the $\delta^{13}\text{C}$ decrease in the mid-depth Atlantic during the last deglaciation, *Earth and Planetary Science Letters*, 571, 117106, <https://doi.org/10.1016/j.epsl.2021.117106>, 2021.
- 725 Hasumi, H.: CCSR Rep. 25, chap. CCSR Ocean Component Model (COCO) Version 4.0, p. 103 pp., Center for Climate System Research, Univ. of Tokyo, Japan, 2006.
- He, F., Shakun, J. D., Clark, P. U., Carlson, A. E., Liu, Z., Otto-Bliesner, B. L., and Kutzbach, J. E.: Northern Hemisphere forcing of Southern Hemisphere climate during the last deglaciation, *Nature*, 494, 81–85, <https://doi.org/10.1038/nature11822>, 2013.
- 730 Howe, J. N. W., Piotrowski, A. M., Noble, T. L., Mulitza, S., Chiessi, C. M., and Bayon, G.: North Atlantic Deep Water Production during the Last Glacial Maximum, *Nature Communications*, 7, <https://doi.org/10.1038/ncomms11765>, 2016.
- Ivanovic, R. F., Gregoire, L. J., Kageyama, M., Roche, D. M., Valdes, P. J., Burke, A., Drummond, R., Peltier, W. R., and Tarasov, L.: Transient climate simulations of the deglaciation 21–9 thousand years before present (version 1) – PMIP4 Core experiment design and boundary conditions, *Geoscientific Model Development*, 9, 2563–2587, <https://doi.org/10.5194/gmd-9-2563-2016>, 2016.
- 735 Ivanovic, R. F., Gregoire, L. J., Burke, A., Wickert, A. D., Valdes, P. J., Ng, H. C., Robinson, L. F., McManus, J. F., Mitrovica, J. X., Lee, L., and Dentith, J. E.: Acceleration of Northern Ice Sheet Melt Induces AMOC Slowdown and Northern Cooling in Simulations of the Early Last Deglaciation, *Paleoceanography and Paleoclimatology*, 33, 807–824, <https://doi.org/10.1029/2017pa003308>, 2018.
- Jeltsch-Thömmes, A., Battaglia, G., Cartapanis, O., Jaccard, S. L., and Joos, F.: Low terrestrial carbon storage at the Last Glacial Maximum: constraints from multi-proxy data, *Climate of the Past*, 15, 849–879, <https://doi.org/10.5194/cp-15-849-2019>, 2019.
- 740 Jochum, M., Chase, Z., Nuterman, R., Pedro, J., Rasmussen, S., Vettoretti, G., and Zheng, P.: Carbon Fluxes during Dansgaard–Oeschger Events as Simulated by an Earth System Model, *Journal of Climate*, 35, 5745–5758, <https://doi.org/10.1175/jcli-d-21-0713.1>, 2022.
- Jouzel, J., Masson-Delmotte, V., Cattani, O., Dreyfus, G., Falourd, S., Hoffmann, G., Minster, B., Nouet, J., Barnola, J. M., Chappellaz, J., Fischer, H., Gallet, J. C., Johnsen, S., Leuenberger, M., Loulergue, L., Luethi, D., Oerter, H., Parrenin, F., Raisbeck, G., Raynaud, D., Schilt, A., Schwander, J., Selmo, E., Souchez, R., Spahni, R., Stauffer, B., Steffensen, J. P., Stenni, B., Stocker, T. F., Tison, J. L., 745 Werner, M., and Wolff, E. W.: Orbital and Millennial Antarctic Climate Variability over the Past 800,000 Years, *Science*, 317, 793–796, <https://doi.org/10.1126/science.1141038>, 2007.

- K-1 Model Developers: K-1 Tech. Rep. 1, chap. K-1 Coupled GCM (MIROC) Description, p. 34 pp., Center for Climate System Research, Univ. of Tokyo, Japan, 2004.
- 750 Kapsch, M.-L., Mikolajewicz, U., Ziemen, F., and Schannwell, C.: Ocean Response in Transient Simulations of the Last Deglaciation Dominated by Underlying Ice-Sheet Reconstruction and Method of Meltwater Distribution, *Geophysical Research Letters*, 49, <https://doi.org/10.1029/2021gl096767>, 2022.
- Kawasaki, T., Matsumura, Y., and Hasumi, H.: Deep water pathways in the North Pacific Ocean revealed by Lagrangian particle tracking, *Scientific Reports*, 12, <https://doi.org/10.1038/s41598-022-10080-8>, 2022.
- 755 Key, R. M., Kozyr, A., Sabine, C. L., Lee, K., Wanninkhof, R., Bullister, J. L., Feely, R. A., Millero, F. J., Mordy, C., and Peng, T.-H.: A global ocean carbon climatology: Results from Global Data Analysis Project (GLODAP), *Global Biogeochemical Cycles*, 18, GB4031, <https://doi.org/10.1029/2004gb002247>, 2004.
- Kobayashi, H., Oka, A., Yamamoto, A., and Abe-Ouchi, A.: Glacial carbon cycle changes by Southern Ocean processes with sedimentary amplification, *Science Advances*, 7, <https://doi.org/10.1126/sciadv.abg7723>, 2021.
- 760 Kohfeld, K. E. and Chase, Z.: Controls on deglacial changes in biogenic fluxes in the North Pacific Ocean, *Quaternary Science Reviews*, 30, 3350–3363, <https://doi.org/10.1016/j.quascirev.2011.08.007>, 2011.
- Kurahashi-Nakamura, T., Paul, A., and Losch, M.: Dynamical reconstruction of the global ocean state during the Last Glacial Maximum, *Paleoceanography*, 32, 326–350, <https://doi.org/10.1002/2016pa003001>, 2017.
- Lhardy, F., Bouttes, N., Roche, D. M., Abe-Ouchi, A., Chase, Z., Crichton, K. A., Ilyina, T., Ivanovic, R., Jochum, M., Kageyama, M., Kobayashi, H., Liu, B., Menviel, L., Muglia, J., Nuterman, R., Oka, A., Vettoretti, G., and Yamamoto, A.: A First Intercomparison of the 765 Simulated LGM Carbon Results Within PMIP-Carbon: Role of the Ocean Boundary Conditions, *Paleoceanography and Paleoclimatology*, 36, e2021PA004 302, <https://doi.org/10.1029/2021pa004302>, 2021.
- Li, C., Clementi, V. J., Bova, S. C., Rosenthal, Y., Childress, L. B., Wright, J. D., and and, Z. J.: The Sediment Green-Blue Color Ratio as a Proxy for Biogenic Silica Productivity Along the Chilean Margin, *Geochemistry, Geophysics, Geosystems*, 23, <https://doi.org/10.1029/2022gc010350>, 2022.
- 770 Lippold, J., Luo, Y., Francois, R., Allen, S. E., Gherardi, J., Pichat, S., Hickey, B., and Schulz, H.: Strength and geometry of the glacial Atlantic Meridional Overturning Circulation, *Nature Geoscience*, 5, 813–816, <https://doi.org/10.1038/ngeo1608>, 2012.
- Liu, Z., Otto-Bliesner, B. L., He, F., Brady, E. C., Tomas, R., Clark, P. U., Carlson, A. E., Lynch-Stieglitz, J., Curry, W., Brook, E., Erickson, D., Jacob, R., Kutzbach, J., and Cheng, J.: Transient Simulation of Last Deglaciation with a New Mechanism for Bølling-Allerød Warming, *Science*, 325, 310–314, <https://doi.org/10.1126/science.1171041>, 2009.
- 775 Locarnini, R. A., O'Brien, T. D., Garcia, H. E., Antonov, J. I., Boyer, T. P., Conkright, M. E., and Stephens, C.: *World Ocean Atlas 2001*, vol. 3, Oxygen, NOAA Atlas NESDIS, vol. 51, p. 286 pp., NOAA, Silver Spring, Md., 2002.
- Lunt, D. J., Williamson, M. S., Valdes, P. J., Lenton, T. M., and Marsh, R.: Comparing transient, accelerated, and equilibrium simulations of the last 30 000 years with the GENIE-1 model, *Climate of the Past*, 2, 221–235, <https://doi.org/10.5194/cp-2-221-2006>, 2006.
- 780 Lüthi, D., Floch, M. L., Bereiter, B., Blunier, T., Barnola, J.-M., Siegenthaler, U., Raynaud, D., Jouzel, J., Fischer, H., Kawamura, K., and Stocker, T. F.: High-resolution carbon dioxide concentration record 650,000–800,000 years before present, *Nature*, 453, 379–382, <https://doi.org/10.1038/nature06949>, 2008.
- Maier, E., Méheust, M., Abelman, A., Gersonde, R., Chaplignin, B., Ren, J., Stein, R., Meyer, H., and Tiedemann, R.: Deglacial subarctic Pacific surface water hydrography and nutrient dynamics and links to North Atlantic climate variability and atmospheric CO₂, *Paleoceanography*, 30, 949–968, <https://doi.org/10.1002/2014pa002763>, 2015.

- 785 Marcott, S. A., Bauska, T. K., Buizert, C., Steig, E. J., Rosen, J. L., Cuffey, K. M., Fudge, T. J., Severinghaus, J. P., Ahn, J., Kalk, M. L., McConnell, J. R., Sowers, T., Taylor, K. C., White, J. W. C., and Brook, E. J.: Centennial-scale changes in the global carbon cycle during the last deglaciation, *Nature*, 514, 616–619, <https://doi.org/10.1038/nature13799>, 2014.
- MARGO Project Members: Constraints on the magnitude and patterns of ocean cooling at the Last Glacial Maximum, *Nature Geoscience*, 2, 127–132, <https://doi.org/10.1038/ngeo411>, 2009.
- 790 Mariotti, V., Paillard, D., Bopp, L., Roche, D. M., and Bouttes, N.: A coupled model for carbon and radiocarbon evolution during the last deglaciation, *Geophysical Research Letters*, 43, 1306–1313, <https://doi.org/10.1002/2015gl067489>, 2016.
- Martin, J. H.: Glacial-interglacial CO₂ change: The Iron Hypothesis, *Paleoceanography*, 5, 1–13, <https://doi.org/10.1029/pa005i001p00001>, 1990.
- Martínez-García, A., Sigman, D. M., Ren, H., Anderson, R. F., Straub, M., Hodell, D. A., Jaccard, S. L., Eglinton, T. I., and Haug, G. H.:
795 Iron Fertilization of the Subantarctic Ocean During the Last Ice Age, *Science*, 343, 1347–1350, <https://doi.org/10.1126/science.1246848>, 2014.
- McManus, J. F., Francois, R., Gherardi, J.-M., Keigwin, L. D., and Brown-Leger, S.: Collapse and rapid resumption of Atlantic meridional circulation linked to deglacial climate changes, *Nature*, 428, 834–837, <https://doi.org/10.1038/nature02494>, 2004.
- Menviel, L., Timmermann, A., Mouchet, A., and Timm, O.: Climate and marine carbon cycle response to changes in the strength of the
800 Southern Hemispheric westerlies, *Paleoceanography*, 23, <https://doi.org/10.1029/2008pa001604>, 2008.
- Menviel, L., Timmermann, A., Timm, O. E., and Mouchet, A.: Deconstructing the Last Glacial termination: the role of millennial and orbital-scale forcings, *Quaternary Science Reviews*, 30, 1155–1172, <https://doi.org/10.1016/j.quascirev.2011.02.005>, 2011.
- Menviel, L., Joos, F., and Ritz, S.: Simulating atmospheric CO₂, ¹³C and the marine carbon cycle during the Last Glacial–Interglacial cycle: possible role for a deepening of the mean remineralization depth and an increase in the oceanic nutrient inventory, *Quaternary Science
805 Reviews*, 56, 46–68, <https://doi.org/10.1016/j.quascirev.2012.09.012>, 2012.
- Menviel, L., England, M. H., Meissner, K. J., Mouchet, A., and Yu, J.: Atlantic-Pacific seesaw and its role in outgassing CO₂ during Heinrich events, *Paleoceanography*, 29, 58–70, <https://doi.org/10.1002/2013pa002542>, 2014.
- Menviel, L., Yu, J., Joos, F., Mouchet, A., Meissner, K. J., and England, M. H.: Poorly ventilated deep ocean at the Last Glacial Maximum inferred from carbon isotopes: A data-model comparison study, *Paleoceanography*, 32, 2–17, <https://doi.org/10.1002/2016pa003024>, 2017.
- 810 Menviel, L., Spence, P., Yu, J., Chamberlain, M. A., Matear, R. J., Meissner, K. J., and England, M. H.: Southern Hemisphere westerlies as a driver of the early deglacial atmospheric CO₂ rise, *Nature Communications*, 9, <https://doi.org/10.1038/s41467-018-04876-4>, 2018.
- Millero, F. J.: Thermodynamics of the carbon dioxide system in the oceans, *Geochimica et Cosmochimica Acta*, 59, 661–677, [https://doi.org/10.1016/0016-7037\(94\)00354-o](https://doi.org/10.1016/0016-7037(94)00354-o), 1995.
- Muglia, J., Skinner, L. C., and Schmittner, A.: Weak overturning circulation and high Southern Ocean nutrient utilization maximized glacial
815 ocean carbon, *Earth and Planetary Science Letters*, 496, 47–56, <https://doi.org/10.1016/j.epsl.2018.05.038>, 2018.
- Muglia, J., Mulitza, S., Repschläger, J., Schmittner, A., Lembke-Jene, L., Lisiecki, L., Mix, A., Saraswat, R., Sikes, E., Waelbroeck, C., Gottschalk, J., Lippold, J., Lund, D., Martinez-Mendez, G., Michel, E., Muschitiello, F., Naik, S., Okazaki, Y., Stott, L., Voelker, A., and Zhao, N.: A global synthesis of high-resolution stable isotope data from benthic foraminifera of the last deglaciation, *Scientific Data*, 10, <https://doi.org/10.1038/s41597-023-02024-2>, 2023.
- 820 Ng, H. C., Robinson, L. F., McManus, J. F., Mohamed, K. J., Jacobel, A. W., Ivanovic, R. F., Gregoire, L. J., and Chen, T.: Coherent deglacial changes in western Atlantic Ocean circulation, *Nature Communications*, 9, <https://doi.org/10.1038/s41467-018-05312-3>, 2018.

- Obase, T. and Abe-Ouchi, A.: Abrupt Bölling-Alleröd Warming Simulated under Gradual Forcing of the Last Deglaciation, *Geophysical Research Letters*, 46, 11 397–11 405, <https://doi.org/10.1029/2019gl084675>, 2019.
- Obase, T., Abe-Ouchi, A., and Saito, F.: Abrupt climate changes in the last two deglaciations simulated with different Northern ice sheet discharge and insolation, *Scientific Reports*, 11, <https://doi.org/10.1038/s41598-021-01651-2>, 2021.
- Obase, T., Meniel, L., Abe-Ouchi, A., Vadsaria, T., Ivanovic, R., Snoll, B., Sherriff-Tadano, S., Valdes, P. J., Gregoire, L., Kapsch, M.-L., Mikolajewicz, U., Bouttes, N., Roche, D., Lhardy, F., He, C., Otto-Bliesner, B., and Liu, Z.: Multi-model assessment of the deglacial climatic evolution at high southern latitudes, *Climate of the Past*, Discuss [preprint], <https://doi.org/10.5194/cp-2023-86>, in review, 2023.
- Ohgaito, R., Yamamoto, A., Hajima, T., O'ishi, R., Abe, M., Tatebe, H., Abe-Ouchi, A., and Kawamiya, M.: PMIP4 experiments using MIROC-ES2L Earth system model, *Geoscientific Model Development*, 14, 1195–1217, <https://doi.org/10.5194/gmd-14-1195-2021>, 2021.
- Oka, A. and Niwa, Y.: Pacific deep circulation and ventilation controlled by tidal mixing away from the sea bottom, *Nature Communications*, 4, <https://doi.org/10.1038/ncomms3419>, 2013.
- Okazaki, Y., Timmermann, A., Meniel, L., Harada, N., Abe-Ouchi, A., Chikamoto, M. O., Mouchet, A., and Asahi, H.: Deepwater Formation in the North Pacific During the Last Glacial Termination, *Science*, 329, 200–204, <https://doi.org/10.1126/science.1190612>, 2010.
- O'Leary, M. H.: Carbon isotope fractionation in plants, *Phytochemistry*, 20, 553–567, [https://doi.org/10.1016/0031-9422\(81\)85134-5](https://doi.org/10.1016/0031-9422(81)85134-5), 1981.
- Parekh, P., Follows, M. J., and Boyle, E. A.: Decoupling of iron and phosphate in the global ocean, *Global Biogeochemical Cycles*, 19, GB2020, <https://doi.org/10.1029/2004gb002280>, 2005.
- Paul, A., Mulitza, S., Stein, R., and Werner, M.: A global climatology of the ocean surface during the Last Glacial Maximum mapped on a regular grid (GLOMAP), *Climate of the Past*, 17, 805–824, <https://doi.org/10.5194/cp-17-805-2021>, 2021.
- Petit, J. R., Jouzel, J., Raynaud, D., Barkov, N. I., Barnola, J.-M., Basile, I., Bender, M., Chappellaz, J., Davis, M., Delaygue, G., Delmotte, M., Kotlyakov, V. M., Legrand, M., Lipenkov, V. Y., Lorius, C., Pépin, L., Ritz, C., Saltzman, E., and Stievenard, M.: Climate and atmospheric history of the past 420, 000 years from the Vostok ice core, Antarctica, *Nature*, 399, 429–436, <https://doi.org/10.1038/20859>, 1999.
- Pöppelmeier, F., Jeltsch-Thömmes, A., Lippold, J., Joos, F., and Stocker, T. F.: Multi-proxy constraints on Atlantic circulation dynamics since the last ice age, *Nature Geoscience*, 16, 349–356, <https://doi.org/10.1038/s41561-023-01140-3>, 2023.
- Rae, J. W. B., Sarnthein, M., Foster, G. L., Ridgwell, A., Grootes, P. M., and Elliott, T.: Deep water formation in the North Pacific and deglacial CO₂ rise, *Paleoceanography*, 29, 645–667, <https://doi.org/10.1002/2013pa002570>, 2014.
- Rafter, P. A., Gray, W. R., Hines, S. K., Burke, A., Costa, K. M., Gottschalk, J., Hain, M. P., Rae, J. W., Southon, J. R., Walczak, M. H., Yu, J., Adkins, J. F., and DeVries, T.: Global reorganization of deep-sea circulation and carbon storage after the last ice age, *Science Advances*, 8, <https://doi.org/10.1126/sciadv.abq5434>, 2022.
- Reimer, P. J., Austin, W. E. N., Bard, E., Bayliss, A., Blackwell, P. G., Ramsey, C. B., Butzin, M., Cheng, H., Edwards, R. L., Friedrich, M., Grootes, P. M., Guilderson, T. P., Hajdas, I., Heaton, T. J., Hogg, A. G., Hughen, K. A., Kromer, B., Manning, S. W., Muscheler, R., Palmer, J. G., Pearson, C., van der Plicht, J., Reimer, R. W., Richards, D. A., Scott, E. M., Southon, J. R., Turney, C. S. M., Wacker, L., Adolphi, F., Büntgen, U., Capano, M., Fahrni, S. M., Fogtmann-Schulz, A., Friedrich, R., Köhler, P., Kudsk, S., Miyake, F., Olsen, J., Reinig, F., Sakamoto, M., Sookdeo, A., and Talamo, S.: The IntCal20 Northern Hemisphere Radiocarbon Age Calibration Curve (0–55 cal kBP), *Radiocarbon*, 62, 725–757, <https://doi.org/10.1017/rdc.2020.41>, 2020.
- Schmitt, J., Schneider, R., Elsig, J., Leuenberger, D., Lourantou, A., Chappellaz, J., Köhler, P., Joos, F., Stocker, T. F., Leuenberger, M., and Fischer, H.: Carbon isotope constraints on the deglacial CO₂ rise from ice cores, *Science*, 336, 711–714, <https://doi.org/10.1126/science.1217161>, 2012.

- 860 Schmittner, A. and Galbraith, E. D.: Glacial greenhouse-gas fluctuations controlled by ocean circulation changes, *Nature*, 456, 373–376, <https://doi.org/10.1038/nature07531>, 2008.
- Schmittner, A. and Lund, D. C.: Early deglacial Atlantic overturning decline and its role in atmospheric CO₂ rise inferred from carbon isotopes ($\delta^{13}\text{C}$), *Climate of the Past*, 11, 135–152, <https://doi.org/10.5194/cp-11-135-2015>, 2015.
- Schmittner, A., Gruber, N., Mix, A. C., Key, R. M., Tagliabue, A., and Westberry, T. K.: Biology and air–sea gas exchange controls on the
865 distribution of carbon isotope ratios ($\delta^{13}\text{C}$) in the ocean, *Biogeosciences*, 10, 5793–5816, <https://doi.org/10.5194/bg-10-5793-2013>, 2013.
- Sherriff-Tadano, S., Abe-Ouchi, A., Yoshimori, M., Ohgaito, R., Vadsaria, T., Chan, W.-L., Hotta, H., Kikuchi, M., Kodama, T., Oka, A., and Suzuki, K.: Southern Ocean Surface Temperatures and Cloud Biases in Climate Models Connected to the Representation of Glacial Deep Ocean Circulation, *Journal of Climate*, 36, 3849–3866, <https://doi.org/10.1175/jcli-d-22-0221.1>, 2023.
- Siegenthaler, U., Stocker, T. F., Monnin, E., Lüthi, D., Schwander, J., Stauffer, B., Raynaud, D., Barnola, J.-M., Fischer, H., Masson-
870 Delmotte, V., and Jouzel, J.: Stable Carbon Cycle–Climate Relationship During the Late Pleistocene, *Science*, 310, 1313–1317, <https://doi.org/10.1126/science.1120130>, 2005.
- Sigman, D. M., Fripiat, F., Studer, A. S., Kemeny, P. C., Martínez-García, A., Hain, M. P., Ai, X., Wang, X., Ren, H., and Haug, G. H.: The Southern Ocean during the ice ages: A review of the Antarctic surface isolation hypothesis, with comparison to the North Pacific, *Quaternary Science Reviews*, 254, 106732, <https://doi.org/10.1016/j.quascirev.2020.106732>, 2021.
- 875 Sikes, E. L., Umling, N. E., Allen, K. A., Ninnemann, U. S., Robinson, R. S., Russell, J. L., and Williams, T. J.: Southern Ocean glacial conditions and their influence on deglacial events, *Nature Reviews Earth & Environment*, 4, 454–470, <https://doi.org/10.1038/s43017-023-00436-7>, 2023.
- Skinner, L., Primeau, F., Jeltsch-Thömmes, A., Joos, F., Köhler, P., and Bard, E.: Rejuvenating the ocean: mean ocean radiocarbon, CO₂ release, and radiocarbon budget closure across the last deglaciation, *Climate of the Past*, 19, 2177–2202, <https://doi.org/10.5194/cp-19-2177-2023>, 2023.
880
- Snoll, B., Ivanovic, R., Gregoire, L., Sherriff-Tadano, S., Menviel, L., Obase, T., Abe-Ouchi, A., Bouttes, N., He, C., He, F., Kapsch, M., Mikolajewicz, U., Muglia, J., and Valdes, P.: A multi-model assessment of the early last deglaciation (PMIP4 LDv1): The meltwater paradox reigns supreme, <https://doi.org/10.5194/egusphere-2023-1802>, 2023.
- Stein, K., Timmermann, A., Kwon, E. Y., and Friedrich, T.: Timing and magnitude of Southern Ocean sea ice/carbon cycle feedbacks, *Proceedings of the National Academy of Sciences*, 117, 4498–4504, <https://doi.org/10.1073/pnas.1908670117>, 2020.
885
- Studer, A. S., Sigman, D. M., Martínez-García, A., Benz, V., Winckler, G., Kuhn, G., Esper, O., Lamy, F., Jaccard, S. L., Wacker, L., Oleynik, S., Gersonde, R., and Haug, G. H.: Antarctic Zone nutrient conditions during the last two glacial cycles, *Paleoceanography*, 30, 845–862, <https://doi.org/10.1002/2014pa002745>, 2015.
- Stuiver, M., Quay, P. D., and Oslund, H. G.: Abyssal Water Carbon-14 Distribution and the Age of the World Oceans, *Science*, 219, 849–851, <https://doi.org/10.1126/science.219.4586.849>, 1983.
890
- Takemura, T.: Simulation of climate response to aerosol direct and indirect effects with aerosol transport-radiation model, *Journal of Geophysical Research*, 110, D02202, <https://doi.org/10.1029/2004jd005029>, 2005.
- Thiagarajan, N. and McManus, J. F.: Productivity and sediment focusing in the Eastern Equatorial Pacific during the last 30,000 years, *Deep Sea Research Part I: Oceanographic Research Papers*, 147, 100–110, <https://doi.org/10.1016/j.dsr.2019.03.007>, 2019.
- 895 Tierney, J. E., Zhu, J., King, J., Malevich, S. B., Hakim, G. J., and Poulsen, C. J.: Glacial cooling and climate sensitivity revisited, *Nature*, 584, 569–573, <https://doi.org/10.1038/s41586-020-2617-x>, 2020.

- Timm, O. and Timmermann, A.: Simulation of the Last 21 000 Years Using Accelerated Transient Boundary Conditions, *Journal of Climate*, 20, 4377–4401, <https://doi.org/10.1175/jcli4237.1>, 2007.
- 900 Tschumi, T., Joos, F., Gehlen, M., and Heinze, C.: Deep ocean ventilation, carbon isotopes, marine sedimentation and the deglacial CO₂ rise, *Climate of the Past*, 7, 771–800, <https://doi.org/10.5194/cp-7-771-2011>, 2011.
- Uemura, R., Motoyama, H., Masson-Delmotte, V., Jouzel, J., Kawamura, K., Goto-Azuma, K., Fujita, S., Kuramoto, T., Hirabayashi, M., Miyake, T., Ohno, H., Fujita, K., Abe-Ouchi, A., Iizuka, Y., Horikawa, S., Igarashi, M., Suzuki, K., Suzuki, T., and Fujii, Y.: Asynchrony between Antarctic temperature and CO₂ associated with obliquity over the past 720, 000 years, *Nature Communications*, 9, 961, <https://doi.org/10.1038/s41467-018-03328-3>, 2018.
- 905 Weber, M. E.: Antiphased dust deposition and productivity in the Antarctic Zone over 1.5 million years, <https://doi.org/10.1594/PANGAEA.939650>, 2021.
- Wilmes, S.-B., Green, J. A. M., and Schmittner, A.: Enhanced vertical mixing in the glacial ocean inferred from sedimentary carbon isotopes, *Communications Earth & Environment*, 2, <https://doi.org/10.1038/s43247-021-00239-y>, 2021.
- 910 Zhao, N., Marchal, O., Keigwin, L., Amrhein, D., and Gebbie, G.: A Synthesis of Deglacial Deep-Sea Radiocarbon Records and Their (In)Consistency With Modern Ocean Ventilation, *Paleoceanography and Paleoclimatology*, 33, 128–151, <https://doi.org/10.1002/2017pa003174>, 2018.

Fig01.png

Figure 1. (a) Deglacial changes in the ~~maximum volume transport of the~~ Atlantic Meridional Overturning Circulation (AMOC; Sverdrup) with $^{231}\text{Pa}/^{230}\text{Th}$ reconstructed from Bermuda Rise sediment core data ~~at the Bermuda Rise (McManus et al., 2004)~~ (McManus et al., 2004) and compiled sediment core data ~~in from~~ the North Atlantic (~~Ng et al. (Ng et al., 2018). , 2018)~~ (Ng et al., 2018). The strength of the AMOC is defined as the maximum meridional volume transport between 30°N and 90°N at depths below 500 m. (b) Deglacial changes in sea surface temperature (SST) in the Southern Ocean (°C) and the difference in SST from the present day (ΔT_{source}) (~~Uemura et al., 2018~~) (Uemura et al., 2018). (c) Deglacial changes in global mean ocean temperature (MOT; °C) and the difference in MOT from the present day ("Mix²²" of ~~Bereiter et al., 2018~~ Bereiter et al. (2018)). The model output computed by the AOGCM (OA19) (~~Obase and Abe-Ouchi, 2019~~) (Obase and Abe-Ouchi, 2019), shown by blue lines, is compared to reconstructions from geological data, shown by gray lines. The right axes relate to the model output and the left axes relate to the reconstructions.

Fig02.png

Figure 2. (a) Deglacial changes in $\Delta^{14}\text{C}-\text{CO}_2$ (‰) in the atmosphere (solid line) with the reconstruction of IntCal20 (dashed line; [Reimer et al., 2020](#)[Reimer et al. \(2020\)](#)). (b–e) Deglacial changes in $\Delta\Delta^{14}\text{C}$ (‰), difference in $\Delta^{14}\text{C}$ (‰) between the ocean and the atmosphere, averaged in the mid-depth (500–2000 m; blue solid [lines](#)) and deep global ocean (2000–5500 m; red solid [lines](#)) ~~of the~~ Atlantic Ocean (40°S–90°N), Pacific Ocean (40°S–90°N), and ~~the~~ Southern Ocean (90°–40°S) with compiled sediment core data (dashed [lines](#)) of [Rafter et al. \(2022\)](#)[Rafter et al., 2022](#). (f) Deglacial changes in $\delta^{13}\text{C}-\text{CO}_2$ (‰) in the atmosphere (solid line) with the reconstruction (dashed line; [Schmitt et al., 2012](#)[Schmitt et al. \(2012\)](#)). (g–i) Same as (b–e), respectively, except for $\delta^{13}\text{C}$ (‰) with compiled sediment core data of [Muglia et al. \(2023\)](#)[Muglia et al. \(2023\)](#). (k) Deglacial changes in atmospheric $p\text{CO}_2$ (ppm; solid line) with ice core data (dashed line; [Bauska et al., 2021](#)[Bauska et al. \(2021\)](#)). (l–o) Same as (b–e), respectively, except for dissolved inorganic carbon (DIC; mmol m^{-3}). [LGM](#): Last Glacial Maximum, [HS1](#): Heinrich Stadial 1, [BA](#): Bølling–Allerød period, [YD](#): Younger Dryas period. The triangles represent the values reported in [Kobayashi et al. \(2021\)](#)[Kobayashi et al. \(2021\)](#), with the output of PI_sed plotted at the time of 11 [kaBP](#) [ka BP](#) and the output of LGM_all plotted at the time of 21 [kaBP](#) [ka BP](#). [PI_sed](#) is an ocean carbon cycle model experiment conducted under preindustrial forcing, including carbonate sedimentation processes. [LGM_all](#) is an ocean carbon cycle model experiment conducted under LGM forcing, including enhanced salinity stratification in the Southern Ocean, iron fertilization from glaciogenic dust, and carbonate sedimentation processes.

Fig03.png

Figure 3. Oceanic zonal mean distribution of $\Delta\Delta^{14}\text{C}$ (‰), which represents the difference in $\Delta^{14}\text{C}$ between the ocean and the atmosphere, during key periods of the last deglaciation in the Atlantic and Pacific oceans. The specific periods of interest include (a) the Last Glacial Maximum (21 kaBP), (b) Heinrich Stadial 1 (17 kaBP), (c) just before the Bølling-Allerød (BA) transition (15 kaBP), (d) the Bølling-Allerød (BA) warm period (13 kaBP), (e) the Younger Dryas period (12 kaBP), and (f) the Holocene (11 kaBP). The contour interval is 40‰. The sediment core records used in the figure are compiled in Rafter et al. (2022). Model results are averaged over 200 years, i.e., 100 years before and after each target year. However, for 21 kaBP, the average is taken from results spanning 21.0–20.9 kaBP; for 11 kaBP, the average is taken from results spanning 11.1–11.0 kaBP. The figure also includes a compilation of sediment core records where reconstructed values are plotted for 250 years before and after the each target year. The vertical section represents all data within the relevant ocean basins. The abbreviations for the oceans are ATL for Atlantic Ocean, SO for Southern Ocean, and PAC for Pacific Ocean. The top-right notes indicate the number of data points, model–data correlation coefficients, and the root mean square error (RMSE) for both the Atlantic and the Pacific basins.




Fig04.png

Figure 4. Oceanic zonal mean distribution of $\delta^{13}\text{C}$ (‰) during the last deglaciation in the Atlantic and Pacific oceans. The contour interval is 0.25‰. The sediment core records used in the figure are compiled in [Muglia et al. \(2023\)](#) [Muglia et al. \(2023\)](#). The period over which the model output is averaged is ~~+100 years~~-100 years before and after the year of interest. The reconstructed values are also plotted for ~~+100 years~~ 100 years before and after the year of interest.

Fig05.png

Figure 5. (a) Temporal changes in the partial pressure of sea surface CO₂ ($p\text{CO}_2^{\text{os}}$; ppm; gray) during Heinrich Stadial 1 (HS1; differences between 18 and 15 kaBP). The contributions of changes in temperature and salinity (purple), temperature (red), salinity (yellow), dissolved inorganic carbon (DIC) and alkalinity (cyan), DIC (green), and alkalinity (blue) to the changes in $p\text{CO}_2^{\text{os}}$ are shown. The thin gray line shows the time series of the AMOC strength. (b) Temporal changes in the partial pressure of atmospheric $p\text{CO}_2$ and $p\text{CO}_2^{\text{os}}$ (ppm) during HS1. The contributions of changes in temperature and salinity, temperature, salinity, DIC and alkalinity, DIC, and alkalinity to the changes in $p\text{CO}_2^{\text{os}}$ are represented by different colored bars. (c) and (d) Similar to (a) and (b), respectively, but for the Bølling-Allerød period (differences between 15 and 13 kaBP). (e) and (f) Similar to (a) and (b), respectively, but for the Younger Dryas period (differences between 13 and 12 kaBP).

Fig06.png

Figure 6. (a) Changes in partial pressure of sea surface CO₂ ($p\text{CO}_2^{\text{ss}}$; ppm) between the early and late Heinrich Stadial 1 (differences between 15 and 18 ka BP). Changes in $p\text{CO}_2^{\text{ss}}$ attributable solely to changes in (b) temperature and salinity and (c) dissolved inorganic carbon (DIC) and alkalinity, and to changes in sea surface (d) temperature, (e) DIC, and (f) alkalinity between the same periods.

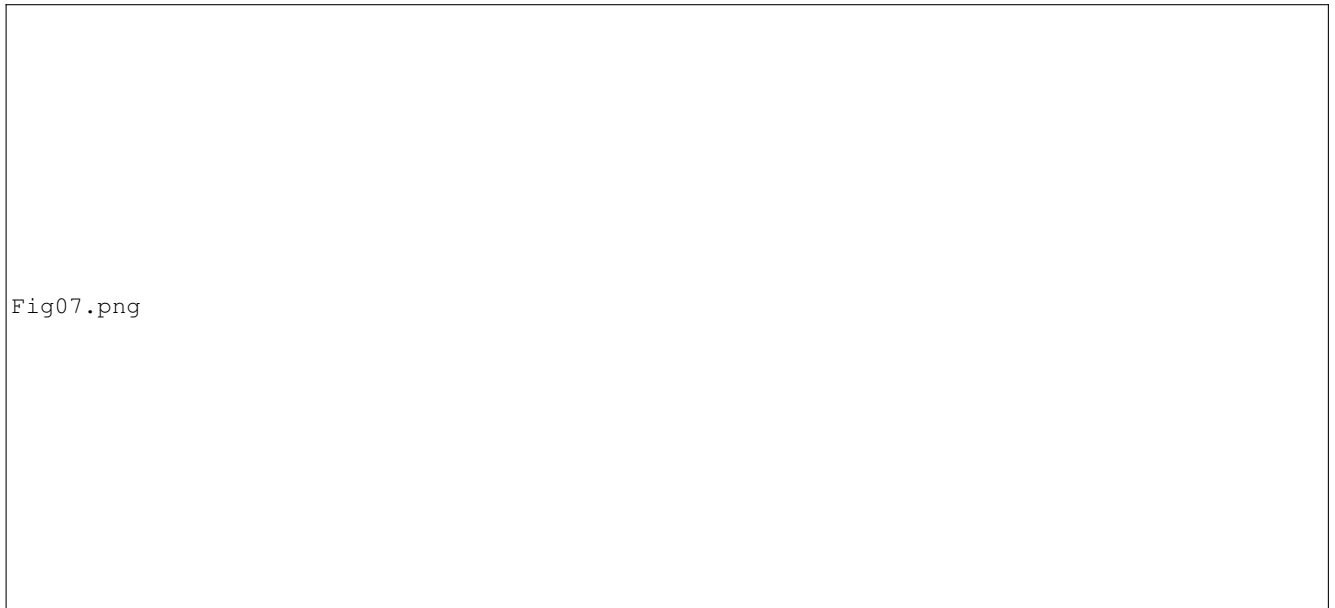


Figure 7. Same as Fig. 6 except for the Bølling–Allerød period (differences between 13 and 15 ka BP).

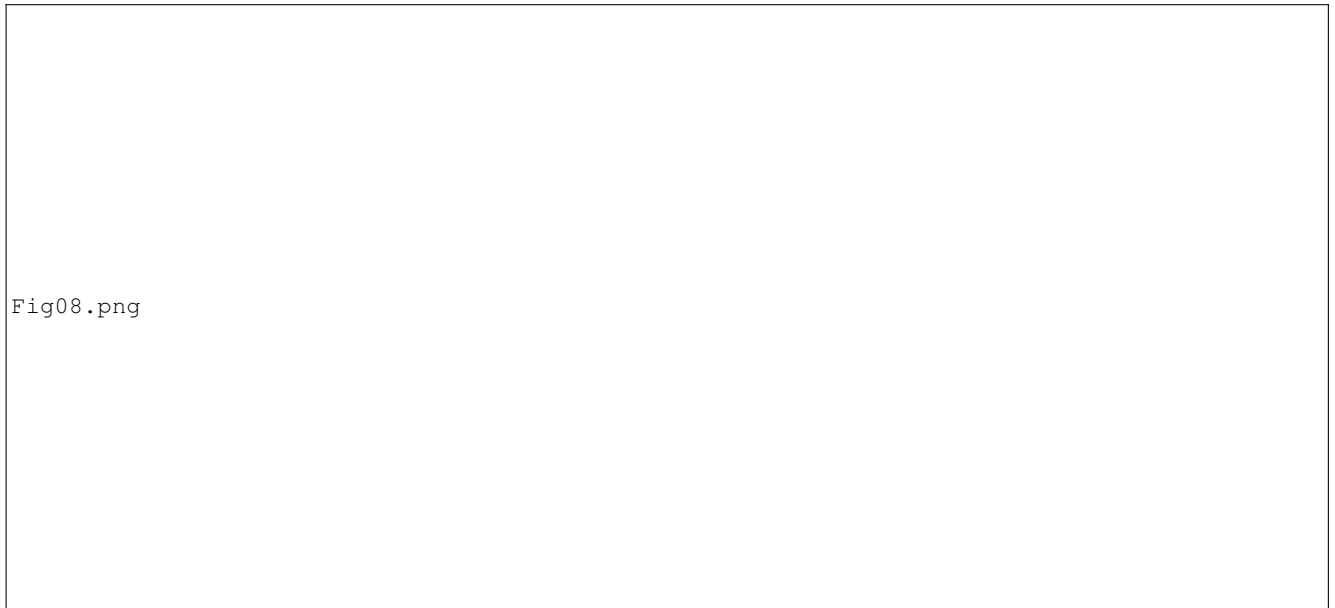


Figure 8. Same as Fig. 6 except for the Younger Dryas period (differences between 12 and 13 ka BP).